

Evaluation and validation of the spectral linear wave theory and ‘traditional’ formulae for pulsating wave loads for unimodal and bimodal seas

Henry Tuin¹, Bas Hofland², Hessel Voortman³, Ermano de Almeida⁴

Abstract

Pulsating wave forces need to be calculated for the design of hydraulic structures. The common formulae are derived for regular or unimodal narrow sea states and use one characteristic wave height and period. However, broad-banded spectra like bimodal sea states are present at many locations. Moreover, new hydraulic structures like post-Panamax locks have a large vertical surface exposed to wave loads. Swell components are disproportionately contributing to the total wave force compared to short waves. This depth effect for broad-banded or bimodal wave spectra is not considered by the traditional wave formulae. This could result in significant underestimations of wave forces on hydraulic structures.

This paper aims to provide a method to define the wave loads of irregular non-breaking wave fields under any wave spectrum. Spectral linear wave theory (LWT) is used to transform a wave spectrum to a wave force or wave pressure spectrum. The spectral LWT allows direct evaluation of the wave force or pressure for the wave spectra considered within this research. Spectral LWT is compared to the outcome of wave flume experiments with bimodal seas and the other common wave force formulae.

This paper also evaluates the application of the spectral LWT to bimodal wave spectra and evaluates the accuracy and validity of other commonly used wave force formulae. For the typical conditions that occur at hydraulic structures (horizontal bed, intermediate to deep water, non-breaking, and unimodal and bimodal seas) the widely used Goda formula is less applicable. The spectral LWT model more accurately describes the wave pressures and forces found in the flume. Goda is well applicable for the evaluation of the global force for (breaking) waves, structures located on a local berm, narrow wave spectra, values of $k_{ph} < 0.5$.

Keywords

Spectral Linear wave theory, NewWave, Goda, Sainflou, Wave spectrum, Wave force spectrum, bimodal seas, Wave forces, Wave pressures, Significant wave force, Significant wave pressure.

¹Henry.tuin@arcadis.com, Arcadis The Netherlands BV, Amersfoort, The Netherlands

²B.hofland@tudelft.nl, Delft University of Technology, Delft, The Netherlands

³Hessel@hesselvoortman.nl, Hessel Voortman Engineering Consultancy B.V., Nijkerk, The Netherlands

⁴Ermano.dealmeida@arcadis.com, Arcadis The Netherlands BV, Amersfoort, The Netherlands


This paper was submitted on 30 June 2022.

It was accepted after double-blind review on 26 October 2022 and published online on 22 November 2022.

DOI: <https://doi.org/10.48438/jchs.2022.0021>

Cite as: “Tuin, H., Hofland, B., Voortman, H., & de Almeida, E. Spectral linear wave theory for wave loads on walls for bimodal seas: Comparison to Goda and measurements. *Journal of Coastal and Hydraulic Structures.*, 3, p. 21.

<https://doi.org/10.48438/jchs.2022.0021>”

The Journal of Coastal and Hydraulic Structures is a community-based, free, and open access journal for the dissemination of high-quality knowledge on the engineering science of coastal and hydraulic structures. This paper has been written and reviewed with care. However, the authors and the journal do not accept any liability which might arise from use of its contents. Copyright ©2022 by the authors. This journal paper is published under a CC-BY-4.0 license, which allows anyone to redistribute, mix and adapt, as long as credit is given to the authors. 

1 Introduction

1.1 Background

In the Netherlands, bimodal sea states have been observed in the harbour basin of IJmuiden located near Amsterdam. The forced due to bimodal seas have been evaluated for the design of lock gates of the new sea lock (Tuin, 2018). The observed bimodal sea states are a combination of waves entering the basin from sea and locally generated wind waves. In recent projects, the author also observed bimodal sea states in the harbors of Terneuzen (Vlaams Nederlandse Scheldecommissie, 2017) and Oostende (Arcadis the Netherlands BV, 2020). For each project the bimodal sea state has been evaluated to a wave force for the design of lock gates and drive mechanism. Bimodal seas have also been observed near the Eastern Scheldt barrier (Mulder, 1980). Petrova (2011) analyzed the occurrence of bimodal sea states for various locations. She concluded that 16% of the sea states corresponded to a mixed sea for the open North Sea, 22% for the North Atlantic, and between 23 to 26% for the Portuguese coast. Moreover, she concluded that bimodal wave fields are often present for low and moderate sea states. Guedes Soares (2012) analyzed 1468 time series of wave records near the Spanish coast. 21% of the analyzed time series were identified as bimodal. The probability distribution of wave heights in bimodal seas were analyzed. He concluded that the Rayleigh and Weibull distributions yield a good fit in almost all ranges of bimodal seas. More bimodal seas have been observed in the Gulf of Oman (Akbari, 2019, 2020). He represented the swell and wind sea peaks of these bimodal seas by a JONSWAP or Gaussian model.

For engineering purposes, three wave formulae are generally used (USACE, 2011): Quasi-regular linear wave theory (Airy, 1845), second order theory of Sainflou (Sainflou, 1928), and the semi-empirical theory of Goda-Takahashi (Goda, 2010). The formula of Goda-Takahashi consists of many factors to account for the geometry at the hydraulic structure and the occurrence of impulsive wave forces. Goda-Takahashi has been derived for the global stability (sliding and overturning) of breakwaters. Each formula uses a single characteristic wave height and a single wave period and is applicable to regular waves and unimodal seas of narrow banded wave spectra. The use and the limitations of Goda-Takahashi has been described in more detail in section 1.2. As stated earlier, sea states are often not classified as narrow banded sea states. To account for the spectral shape, the Spectral LWT (Mulder, 1980) (Tuin, 2018), NewWave theory (Tromans, 1991), and quadratic summation LWT (Van Vledder, 2019) (van Maris 2018) have been developed. These formulae are also described in more detail in section 1.2.

- The main design steps for the evaluation of the force given a design storm are given in Figure 1. The formulae have been subdivided in ‘traditional’ wave force formula, the New Wave, and the Spectral LWT.
- ‘Traditional’ formulae require a single wave height and wave period derived from a wave field or spectrum. A probability distribution is used to scaled to wave height to a design wave. This design wave height and wave period is input to a wave force formula like the formula of Goda-Takahashi, LWT, or Sainflou.
- The ‘quadratic summation LWT’ (Van Vledder, 2019) (van Maris 2018) decomposes the wave spectrum and evaluates the wave force of a ‘swell’ component and a ‘sea’ component. Two wave heights and two wave periods are evaluated for a bimodal sea.
- The New Wave approach (Tromans, 1991) defines a ‘most probable extreme crest shape’ based on a wave spectrum. The most probable crest shape is used for the evaluation of the wave force.
- The Spectral LWT (Mulder, 1980) (Tuin, 2018) uses a response function that is based on the local geometry of the hydraulic structure and transfers the wave spectrum to a wave or pressure spectrum. A significant wave force or pressure is derived and scaled to a design force using a probability distribution. This approach is described in more detail in chapter 2.

Several higher-order wave theories for pulsating wave loads on vertical walls have been formulated based on Stokes-like expansion theories, for third order (Tadibakhsh and Keller, 1960), fourth order (Goda 1967) and fifth order (Penney and Price, 1952; Sobey, 2009). These formulae are not regularly used in practical applications. One reason for this is the lengthy algebraic expressions that have been proven to lead to errors (Sobey, 2009). Moreover, these theories have been derived for regular waves, such that their increased accuracy is clouded by the inaccuracy due to their use for an irregular wave field using a quasi-regular wave assumption.

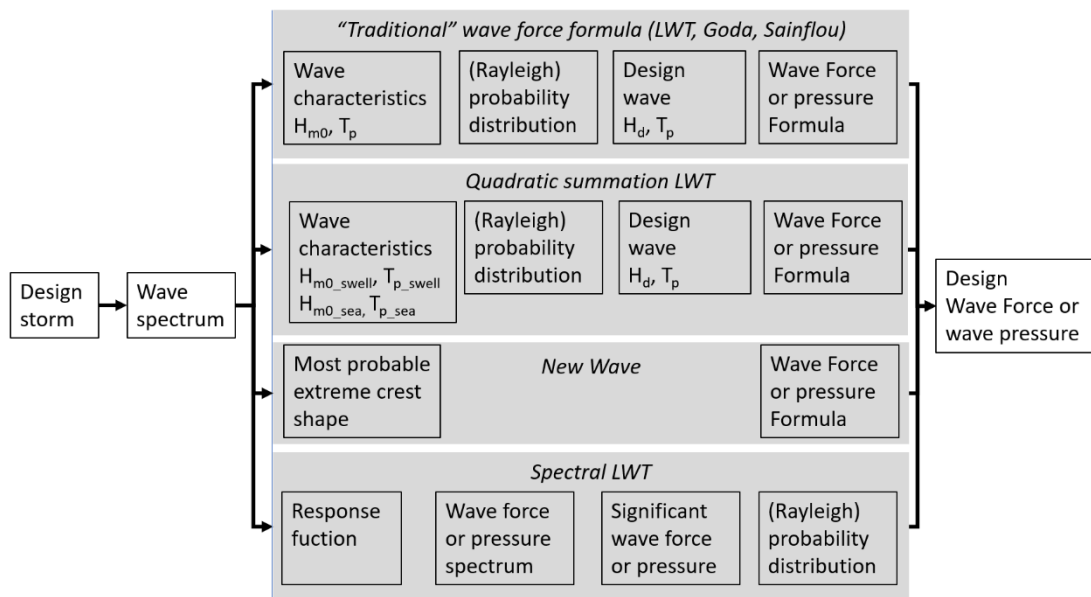


Figure 1: Wave force formula – flow chart

Goda (1966) compared the forces calculated with his fourth-order formula to the peak forces of single extreme waves in an irregular wave field, where he used the zero-downcrossing wave period, and incoming averaged wave height as input for the (regular) wave-theory. Ten wave trains of 15 to 20 irregular waves per train were analyzed. The deviation of the predicted wave force using the fourth-order analytical formula compared to the measured wave force was +/- 25%. Hence, the increased accuracy of the higher order theories does not seem to help to make an accurate prediction of pulsating wave forces in irregular wave fields.

Waves with high steepness (ratio of wave height to wavelength) and/or relative depth (ratio of depth to wavelength) become non-linear and show a ‘double hump’ in the time series of wave heights, pressures, and wave forces. Higher order effects are more prominent when ‘double humps’ are observed at the water level or in the wave force for an increasing wave steepness (Goda, 1966). Recent studies show the ‘double humps’ for wave pressures (Romanczyk, 2007) and water level elevations (Chen Yang-Yih, 2009)

1.2 Goda, Spectral LWT, NewWave and Quadratic LWT

A frequently applied formula for engineering purposes is the formula of Goda (1974, 2010). The Goda formula is derived for the design of caisson breakwaters and considers failure modes like sliding, overturning, and failure of the foundation (Goda, 2010). Before the development of the formula of Goda-Takahashi, caisson breakwaters were designed using the Sainflou formula (Sainflou, 1928) and the Hiroi formula ($p = 1.5\rho gH_d$) (Hiroi, 1919). The formula of Sainflou was used for water depths larger than two times the wave height and the Hiroi formula was applied for water depths smaller than two times the wave height. The formulas of Hiroi and Sainflou are not applicable for depth induced breaking waves due to a berm on which a breakwater is situated. Goda (1972) performed many laboratory tests to derive an improved wave formula which is known as the ‘formula of Goda’ (Goda, 1974, 2010). The laboratory tests were based on:

- Regular waves. The wave period was kept constant during a test. The wave height was increased step by step. Roughly 10 single waves were applied per wave height.
- Relative depths of $h/L = 0.1$ and 0.3 .
- A constant bed slope of $1/100$.

The final Goda-Takahashi (1974, 2010) formula uses the pressure at still water level (SWL) as input parameter for the full pressure profile (from top crest to bottom). It is a rather complicated set of formulae with semi-empirical coefficients for many influences like impulsive wave impacts, oblique waves, sloping bed, and presence of a berm. For

pulsating normally incident waves at structures on a horizontal bed without berm (for structures like sea locks, discharge sluices, or quay walls) the formula for the pressure at SWL reduces to equation 1, as given by Paprota (2021). The alpha factors representing the effect of a berm and impulsive loading are equal to 0.6 for α_1 and 0.0 for α_2 (factor for presence of rubble mound foundation) and α_3 (factor for pressure distribution) (Goda, 1992). These factors are not relevant for the evaluation of the wave force for incident waves and structures on a horizontal bed without berm. Within the research presented in this paper the full set of formulae as presented by Goda (2010) have been applied.

$$p_1 = \left(0.6 + \frac{2k_d h}{\cos^2(2k_d h)} \right) \rho g H_d \quad (1)$$

where k_d is the (local) wave number based on $T_{1/3}$. The pressure profile is assumed to be bilinear. Above the water line the pressure varies between $p = p_1$ for SWL ($z = h$), and $p = 0$ for $z = h + 0.75H_d$. For low structures, the pressure profile is simply truncated at the top of the structure. Below the water line the pressure is assumed to vary between the $p_1/\cosh kh$ at the bed to p_1 at SWL.

Even though the formula was derived for (composite) caisson breakwaters for the global failure modes like sliding and overturning in nearly breaking and breaking waves in intermediate to shallow water conditions (and is very successful for this application) it is also often recommended in manuals for the assessment of hydraulic structures in intermediate to deep non-breaking waves with non-standard spectra for a variety of structures including lock gates (e.g. Rijkswaterstaat, 2018). However, the design of hydraulic structures like locks, sluices, and barriers deviates from the design of caisson breakwaters. For the design of caisson breakwaters, the global stability of key importance. For the design of ship locks, lock gates and drive mechanism of lock gates the shape of the pressure profile is of major importance. The shape of the pressure profile due to wave loading on gates is normative for plate thickness, the distribution of forces during gate motion, required strength, stiffness of girders, and power of the drive mechanism. For structures located in deep water, the pressure profile is even more important because the pressure profile decreases to zero before reaching the bed level. Using the formula of Goda-Takahashi for these hydraulic structures is therefore not always the best choice.

The Spectral LWT for wave forces on vertical face structures was applied for the design of the Eastern Scheldt Barrier in the Netherlands. This mathematical model forms the basis of this paper and is described in further detail in chapter 2. Wave flume experiments were performed showing the validity of the mathematical model up to a (prototype) frequency of 0.2 Hz (Mulder, 1980). The model was applied to evaluate the forces for extreme conditions for bimodal seas. The peak frequencies of the second peak were lower than 0.3 Hz (Mulder, 1980; Vrijling, 1983). The Spectral LWT was also numerically verified and seemed to give reasonable estimates of the forces for low steepness waves ($H/L < 0.092$) for a greater range of wave frequencies (Van Vledder, 2019).

The Spectral LWT has also been applied for the evaluation of bimodal sea states for the design of the design of the sea lock of IJmuiden (Voortman et al. 2017; Tuin, 2018). The spectral LWT was applied to evaluate the wave forces during normal service conditions relevant for the design of the drive mechanism and gate supports (for opening or closing a lock gate) for more moderate wind seas and higher peak frequencies than the ones used for the design of the Eastern Scheldt Barrier. In the IJmuiden case, the harbor basin is deep to accommodate large vessels. The lock gates are completely vertical up to the horizontal bed. Hence, purely pulsating, non-breaking waves will occur. Long waves of a bimodal spectrum have a major contribution to the wave force on structures for an increasing water depth. Tuin (2018) showed that a minor contribution of low frequency waves in the surface elevation spectrum (2% of the total wave energy) caused a significant contribution to the total wave force (approximately 20% of the total wave force variance).

Tromans (1991) derived the New Wave LWT theory. The “New Wave” group produces a description of the extreme wave, originally defined as an extreme crest elevation, for a particular sea frequency spectrum. The New Wave group effectively describes the average shape surrounding the extreme crest as obtained from an infinite number of random seas, and in mathematical terms is equal to the autocorrelation function. It is based on linear superposition of the different modes. It does not use random phases of the spectrum, but assigns a predefined, most-likely, phase. The shape is scaled for a particular crest elevation to give the most probable surface elevation surrounding the crest. Based on this theory and LWT, the force resulting from the pressure below water level can be calculated with the first term of the formulation below. The second term can be added for the part above the water line, assuming hydrostatic pressure.

$$F_{NW} = \rho g h H_d \int \frac{S(f)}{m_0} \frac{\tanh kh}{kh} df + \frac{1}{2} \rho g H_d^2 \quad (2)$$

where ρ is the density of water, g is the gravitational constant, H_d is the design wave, k is the wavenumber, S is the variance spectral density of the modelled irregular wave field, h is the depth, m_0 is the zeroth order moment of the wave spectrum, and f the frequency.

$$F_{LWT,quadratic} = \sqrt{F_{LWT,swell}^2 + F_{LWT,sea}^2} \quad (3)$$

where $F_{LWT,swell}$ is the force due to the swell component of the spectrum and $F_{LWT,sea}$ is the wind sea component of the spectrum.

1.3 Problem, aim, approach, scope, outline

At many locations around the world, bimodal wide banded sea spectra are observed. A bimodal spectrum can be described by two peak frequencies and two wave heights. The general design formulae (Goda, Quasi-regular LWT, Sainflou) are using only one peak period and one wave height. This makes them less applicable for bimodal seas. From the discussed literature above, it seems that there does not exist a well described method to consider arbitrary spectral shapes in the determination of wave loads for (moderate) seas with high peak frequencies for non-breaking waves. The spectral LWT or NewWave theory can be applied for arbitrary shapes of wave spectra; the Spectral LWT has already been applied to the design of the Eastern Scheldt for the lower frequencies in the force signal under extreme conditions. However, the accuracy of a spectral LWT is not known for a large range of conditions.

Unimodal wave spectra can be evaluated by the general design formulae, Spectral LWT, and NewWave theory. However, the accuracy of these formulae depends on the wave height, wave period and water depth. However, formulas, like the formula of Goda-Takahashi, are often applied beyond their validity or required use. This results in an overestimation or underestimation of the wave force or use of a non-representative pressure profile. The pressure profile as calculated by the formula of Goda-Takahashi and Sainflou does not represent the expected pressure profile. Nevertheless, in most cases this works well for the analysis of global stability like sliding and overturning of caisson breakwaters or comparable structures. However, for the design of hydraulic structures like lock gates, discharge gates, and drive mechanism a representative pressure profile is of great importance. The pressure profile is key for the evaluation of the distribution of wave forces to gate supports, design of steel components, and required strength of the gate. Moreover, for deep sea harbors deep water conditions are often valid. The use of Goda-Takahashi and Sainflou (triangular shape of the pressure profile) could result in an overestimation of the wave forces.

This paper aims to formulate and validate an approach to derive pulsating wave loads on vertical walls valid for unimodal, narrow banded, and wide banded wave spectra. Wave pressure distributions below SWL are analyzed in detail to validate design formulae. The pressure distribution above SWL has been schematized as a triangular profile corresponding to the general wave formulae and not been validated in detail. In the conducted wave flume tests only one pressure sensor was available above SWL which is too little to perform a validation of the pressure profile above SWL.

Wave flume tests have been conducted covering unimodal and bimodal wave fields to validate the Spectral LWT. Theoretical response functions useful for the transformation of wave spectra to wave force spectra have been compared with wave force spectra obtained from the wave flume experiments. Results of multiple general wave load formulae are compared to experimental results to assess their applicability for bimodal seas. Moreover, the different approaches are compared to each other for various ranges of relative depth kph , and different contributions of low frequency energy.

The paper is structured as follows: chapter 2 formulates the Spectral LWT. Chapter 3 presents the conducted experiments used to validate the spectral LWT. Chapter 4 presents the validation of the Spectral LWT and a comparison of the general wave formulae to the experimental results. Chapter 5 presents the results and discussion. Chapter 6 presents the conclusions.

2 Spectral LWT for wave forces on a vertical wall

This chapter presented the derivation and theoretical description of the Spectral LWT which are also described in a likewise manner in (Mulder, 1980). The formulae are not widely known. For convenience and readability of this paper, the applied formulae are presented and explained in more detail in this chapter.

In section 2.1, the wave model of the Spectral LWT is explained for the evaluation of wave pressures. In section 2.2 the theory is described for wave forces. The introduction of the significant wave force and significant wave pressures and probability distribution is given in section 2.3.

2.1 Wave pressure

For the spectral LWT, the contribution to the total wave force of every wave component needs to be calculated within the frequency domain. It requires a relationship between two variables which can be treated as a linear system (Holthuijsen, 2007; Mulder, 1980). A response function is derived using a general expression from the linear wave theory. The pressure at an elevation z below water level is calculated using equation 4 (Holthuijsen, 2007). The pressure-response function given in equation 5 for a variable height ‘ z ’ is derived by dividing equation 4 by the wave amplitude.

$$p_{\text{sub}}(f, z) = a(1 + r) \rho g \frac{\cosh kz}{\cosh kh} \quad (4)$$

$$R_{\eta p, \text{sub}}(f, z) = (1 + r) \rho g \frac{\cosh kz}{\cosh kh} \quad (5)$$

where a is the wave amplitude, r is the reflection coefficient, ρ is the density of water, g is the gravitational constant, k is the wave number (function of the wave (mode) frequency), z is elevation relative to the bottom, and h is the water depth

The response function above water level is found by linear interpolation between SWL and the linearized reference amplitude including reflection. The pressure-response function above SWL is shown in equation 6:

$$R_{\eta p, \text{top}}(f, z) = (1 + r) \rho_w g \left(1 - \frac{z - h}{z_{\text{up}} - h} \right) \quad (6)$$

where: z_{up} is equal to $\min(h + (1 + r)a_{\text{ref}}, z_{\text{top}})$, z_{top} is the top-level of the structure that is subjected to waves, z is the vertical level where the pressure is calculated, h is the water depth.

The wave pressure spectrum at a given height z is derived by multiplying the square of the response function as given in equation 5 and equation 6 with the wave spectrum as shown in equation 7:

$$S_{pp}(f, z) = R_{\eta p}(f, z)^2 S_{\eta\eta}(f) \quad (7)$$

where: $S_{pp}(f, z)$ is the wave pressure spectrum ($\text{N}^2/(\text{m}^4\text{Hz})$), $S_{\eta\eta}(f)$ is the wave (water elevation) spectrum (m^2/Hz), and $R_{\eta p}(f, z)$ is the pressure response function (N/m^3). The pressure response function is equal to $R_{\eta p, \text{sub}}(f, z)$ for $h > z \geq 0$ and equal to $R_{\eta p, \text{top}}(f, z)$ for $z_{\text{top}} > z \geq h$.

Pressure response functions below SWL are illustrated in Figure 2 for 8 levels below SWL. The pressure response at SWL is equal for every value of kh because the pressure-reduction in depth is not present at SWL. Every unit of wave variance gives the same proportion of force for every wave frequency. The pressure response at and near the bottom decreases to zero for an increasing value of kh due to the reduction of wave pressure at larger depths for an increasing wave frequency or kh value. In short:

- Low values of kh (low frequencies & long waves) generate at every depth the same value of pressure response.
- For an increasing value of kh (high frequencies & short waves) the waves are not able to penetrate over the full water column. The pressure response at and near the bottom decreases to zero. As indicated in Figure 2 for multiple relative water depths.

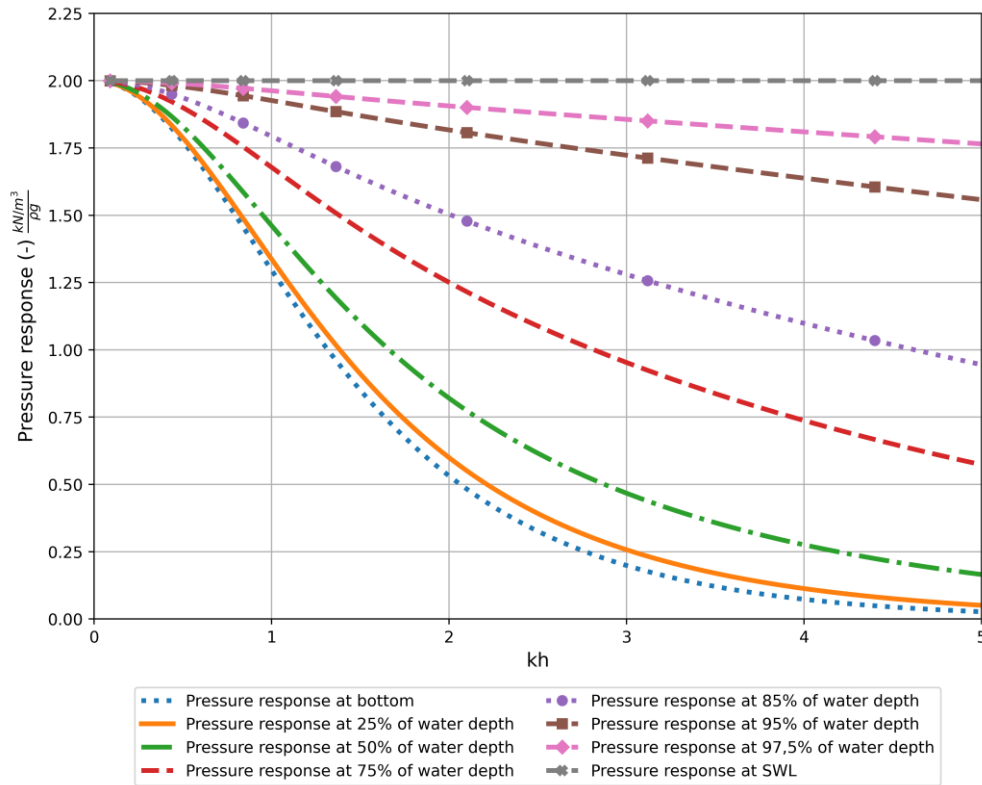


Figure 2: Pressure responses.

2.2 Wave force & response functions

The wave spectrum is transformed to a force spectrum by using the square of the response function as shown in equation 8. The total response function is found by the sum of the response below SWL and above SWL as given in equation 9:

$$S_{FF}(f) = R_{\eta F}^2(f)S_{\eta\eta}(f) \tag{8}$$

where $S_{FF}(f)$ is the wave force spectrum ($N^2/(m^2Hz)$), $S_{\eta\eta}(f)$ the wave (water surface elevation) spectrum (m^2/Hz), and $R_{\eta F}(f)$ the force response function (N/m^2).

$$R_{\eta F}(f) = R_{\eta F_top} + R_{\eta F_sub}(f) \tag{9}$$

The Response function below SWL is a function of wave amplitude, wave frequency, and the water depth over which the wave induces pressure. The response function (equation 10) is derived by dividing the expression of the force from linear wave theory (Airy, 1845) by the wave amplitude:

$$R_{\eta F_sub}(f) = (1 + r) \rho g \int_{z=0}^{h_w} \frac{\cosh kz}{\cosh kh} dz = (1 + r) \rho gh \frac{\tanh kh}{kh} \tag{10}$$

where a is the unreflected wave amplitude, f the frequency, r the reflection coefficient, ρ the water density, g the gravitational constant, k the wave number (as a function of frequency), h the water depth, and z the vertical elevation relative to the bottom.

The response below SWL is illustrated in Figure 3 for multiple water depths for the frequency and kh . The magnitude of the response scales with the water depth. For very low frequencies the hydrostatic force is equal in magnitude over the full depth and the wave forces scales linear over height. For an increasing wave frequency, the depth, and the magnitude of the pressure over which the wave profile penetrates over depth decreases.

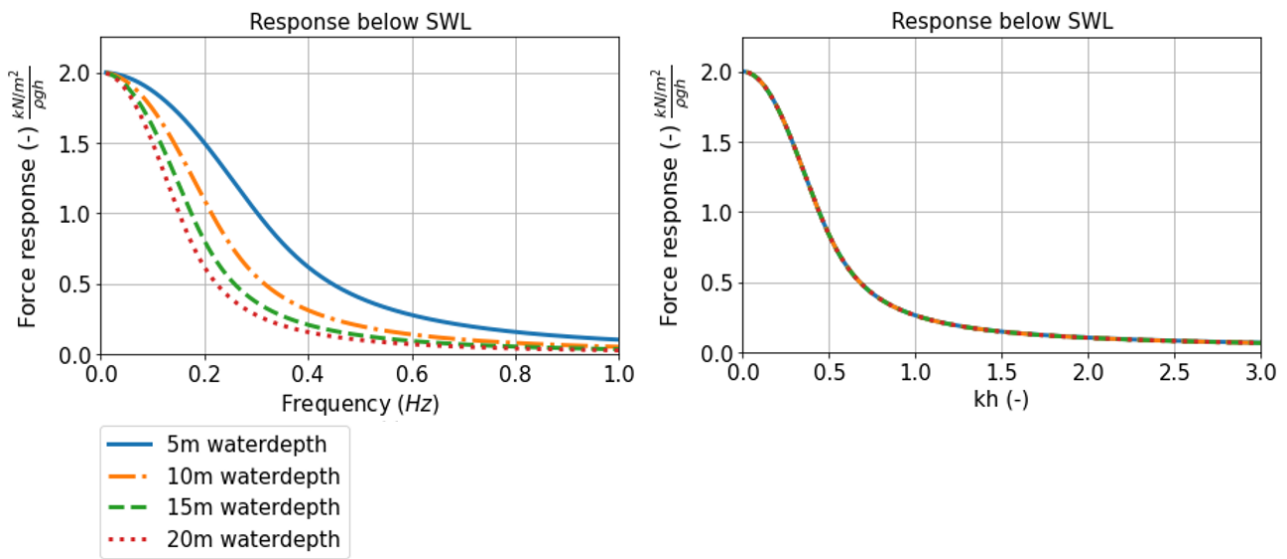


Figure 3: Illustration of force response functions below SWL. Left panel as function of frequency; right panel as function of kh (reflection coefficient = 1).

The pressure profile above water corresponds to a triangle according to the assumption of a hydrostatic pressure distribution for the wave crests above the SWL. Hence a quadratic relation between wave force and wave amplitude is expected for the wave force above SWL, as both the magnitude and height of the pressure profile depends on the wave amplitude. The spectral LWT requires a linear relationship (Holthuijsen, 2007). This is obtained by introducing a reference amplitude as shown in equation 11. The subsequent response function for the force above SWL is given in equation 12. A factor of $\gamma_{lin} = 1.0$ is applied for linearization. This factor is validated in chapter 4. The linearized wave response above SWL is illustrated for four significant wave heights in Figure 4. The linear response is a constant value for every frequency and depends on the magnitude of the reference amplitude and reflection.

$$F_{top} \approx (1 + r)^2 \frac{1}{2} \rho g a_{ref} a \quad (11)$$

where a_{ref} is the reference amplitude = $\frac{1}{2} \gamma_{lin} H_{m0}$, and γ_{lin} a factor.

$$R_{\eta F_{top}} = \frac{F_{top}}{a} = (1 + r)^2 \frac{1}{2} \rho g a_{ref} \quad (12)$$

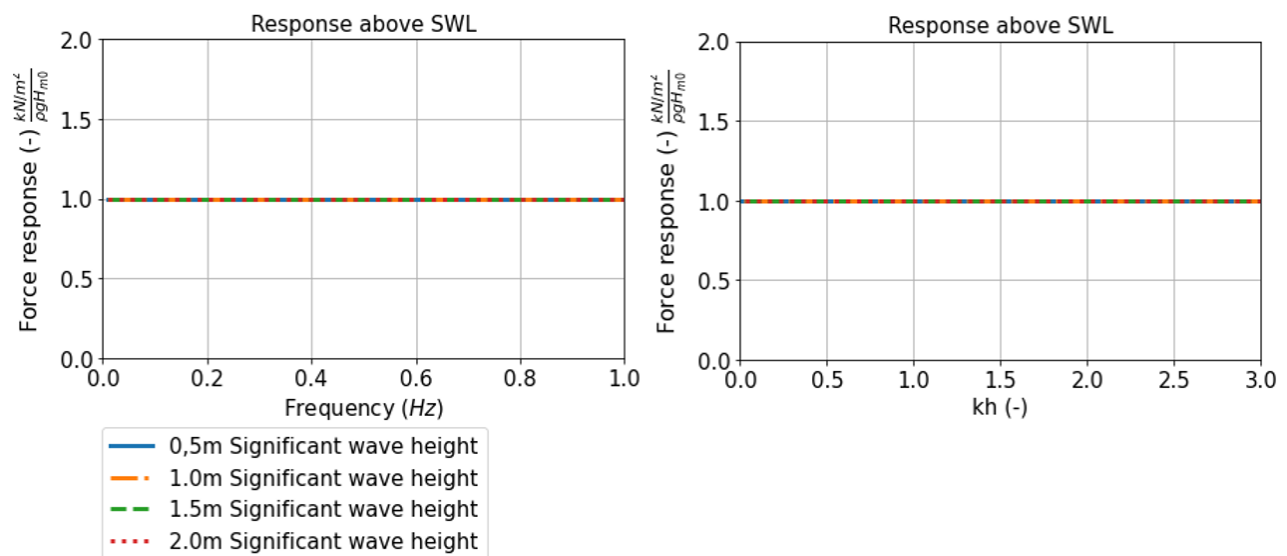


Figure 4: Illustration of force response functions above SWL. Left panel as function of frequency; right panel as function of kh (reflection coefficient = 1).

2.3 Significant wave height, wave force and wave pressure

For the description of wave fields, the wave height H_{m0} is used. The combination of the significant wave height and peak period gives a rather good description of narrow unimodal wave fields (Holthuijsen, 2007). Significant wave forces and pressures can be used to describe the wave loads on structures. The definition of the significant wave force and pressure deviates from the definition of the significant wave height. The wave height is a ‘peak to trough’ value, where for the wave loads it seems more natural to consider only the peak to zero crossing. Hence the significant force or pressure $F_{1/3}$ and $p_{1/3}$ is half the value of that for a trough-peak value. The formula of the significant wave force F_{m0} and pressure $p_{m0}(z)$ based on the zeroth order moment of the spectrum is hence chosen to resemble this significant force and is shown in equation 13 and equation 14 below, respectively. It is not correct to derive F_{m0} by integration of p_{m0} over the depth. This yield in a different order of multiplications of the responses and wave spectra which results in a different result.

$$F_{m0} = 2 \sqrt{m_{0,F}} \quad (13)$$

$$p_{m0}(z) = 2 \sqrt{m_{0,p(z)}} \quad (14)$$

The probability distribution of wave heights in bimodal seas can be described by the Weibull distributions of which the Rayleigh distribution is a special case (Guedes Soares, 2012). The formulation of the Rayleigh distribution is applied for the single zero-crossing wave forces, and pressures, respectively. The Rayleigh distribution is theoretically valid for narrow-banded spectra (Longuet-Higgins, 1952). It therefore needs be validated if this distribution is also valid for bimodal spectra.

$$P_{\text{wave}}(\underline{X} > X) = e^{-2(X/X_s)^2} \quad (15)$$

where X is an arbitrary value representing the wave height, wave force or wave pressure, and X_s is the wave force or wave pressure at a given depth z .

3 Wave flume experiments

3.1 Test setup

Tests have been performed in the wave flume of the Hydraulic Engineering Laboratory of Delft University of Technology. De Almeida (2020) used the flume for the measurements of wave pressures on vertical walls with and without an overhang. Special tests were conducted for bimodal sea states and pressures and forces on vertical walls without an overhang. De Almeida (2020) used a sampling frequency of 20 kHz for his research for the evaluation of impulsive wave loads. The variation of the pressure over time for pulsating loads as discussed in this paper is less compared to wave impact loads. A down sampled dataset with a frequency of 1 kHz is applied in this paper. This down sampled signal was obtained simultaneously to the higher frequency measurement during the tests, by keeping only 1 sample out of 20. No aliasing problems are expected due to the application of low-pass filter with cut-off at 500 Hz. Negligible wave energy is present above 500 Hz.

The test set-up is shown in Figure 5 and Figure 6. The wave height is measured by using three wave gauges located at a distance between 1.515 meter and 2.195 meters from the wall. The method of Zelt and Skjelbreia (1992) is applied to decompose the incident and reflected wave. The weight of the wall was sufficiently large to limit the movements of the wall due to wave loading to increase the accuracy of the measurements. The wave flume time series are used for the validation of the response functions, wave pressures, and probability distributions.

Wave loads have been measured using the pressure sensors which are indicated in Figure 5. Wave pressures were measured at 8 levels. These pressures could directly be related to theoretical pressure profiles. Results of load sensors give an average pressure over the height of the load sensor and cannot be directly related to the theoretical pressure profiles. The pressure sensors are well distributed over the height with a with a closer spacing at the locations where larger pressure gradients are expected, as indicated in Figure 5. A cubic spline is applied using the measurements of PS2, PS3, PS4, PS5, PS6, PS7, and PS9. The wave force is calculated by integration over height. Only one sensor is located just

above SWL which yield to a less accurate estimate of the wave force above SWL. PS10 is located too high and is only loaded by extreme waves within the wave field.

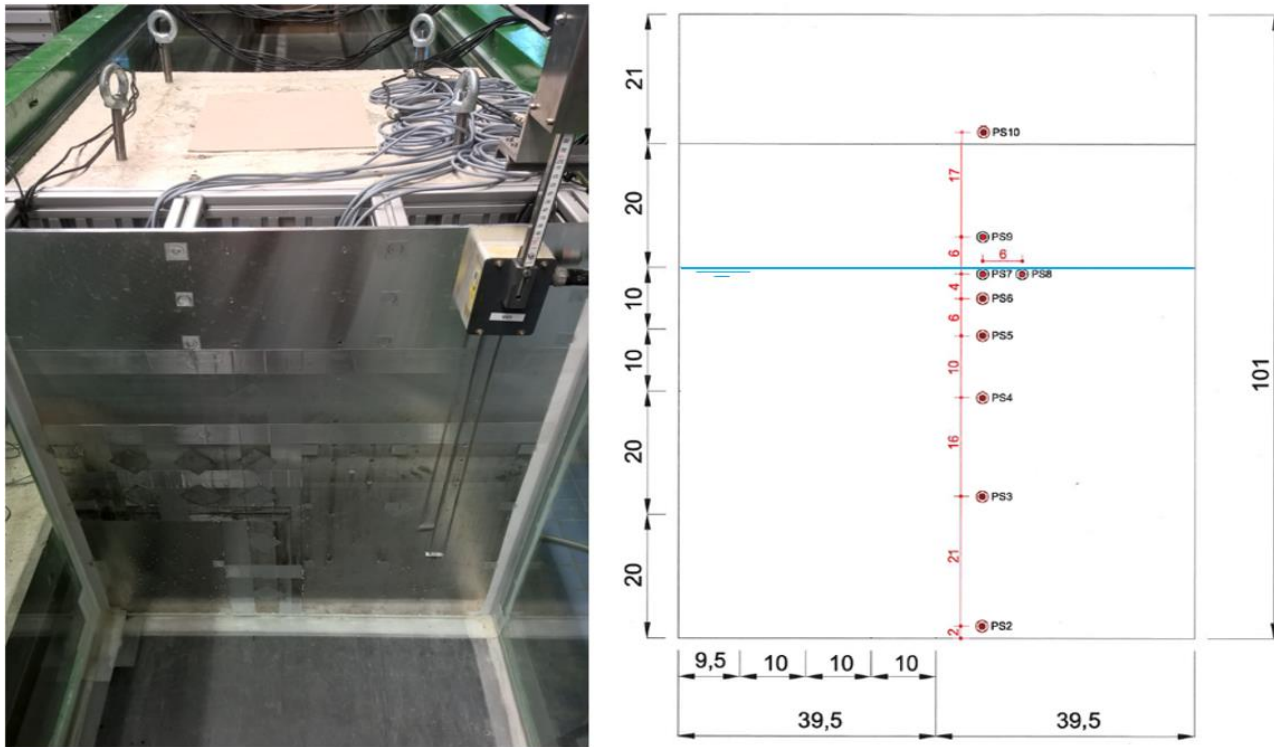


Figure 5: Left: instrumented wall in flume. Right: general layout of wall (based on de Almeida, 2020). Dimensions in cm.

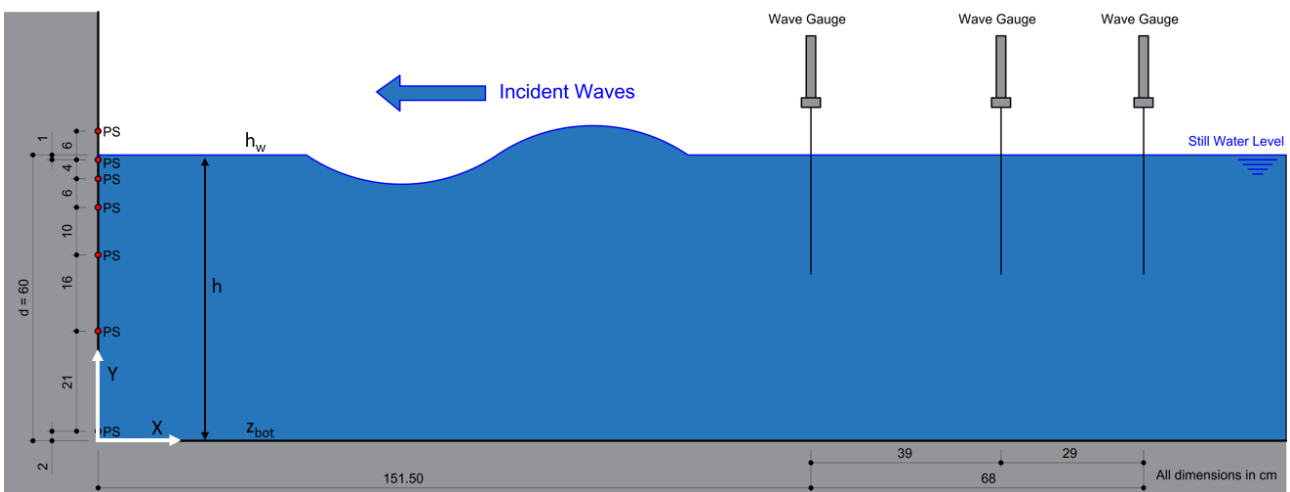


Figure 6: General layout wave flume. Figure based on (de Almeida, 2020).

3.2 Test program

A total of 6 experiments have been analyzed for this paper. Each experiment represents a wave spectrum ranging from a unimodal spectrum to bimodal spectra. The first five experiments were conducted for 20 minutes; experiment 6 lasted for 90 minutes. Table 1 gives an overview of the characteristics of the experiments and applied wave spectra. A water depth of 0.60 m has been applied for every experiment.

Van Maris (2019) implemented two new parameters to describe a bimodal wave spectrum. The parameters are shown in equation 16 and equation 17. The relative swell variance M_{Sw} is defined as the ratio of wave variances of the wind sea

and swell. The relative swell peak frequency Φ_{sw} is based on the ratio of the wind sea peak frequency and swell peak frequency.

$$M_{sw} = \frac{m_{0,swell}}{m_{0,swell} + m_{0,sea}} \quad (16)$$

$$\Phi_{sw} = \frac{f_{p,sea} - f_{p,swell}}{f_{p,sea}} \quad (17)$$

where M_{sw} is the relative swell variance, $m_{0,swell}$ is the swell variance (total variance below the minimum between the swell and wind component), $m_{0,sea}$ is the wind sea variance (total variance above the minimum between both components), Φ_{sw} is the relative swell peak frequency, $f_{p,swell}$ is the peak frequency of the swell spectrum, and $f_{p,sea}$ is the peak frequency of the wind sea spectrum.

The relative swell peak frequency for every experiment has been set at a fixed value of 0.59. The peak frequency has been increased to investigate the effect of the frequency on the transformation of the wave spectrum to the wave force spectrum. The relative swell variance ranges from zero (unimodal wave spectrum) up to a relative swell of 0.55 (bimodal 55% swell variance). The bimodal spectra were generated by adding JONSWAP spectra for the swell spectrum and the wind sea corresponding to the parameters given in Table 1. The wave spectrum and wave force spectrum are derived using a Fast Fourier Transformation. The results are given in chapter 4.

Table 1: Measured wave characteristics in model tests.

Experiment	<i>Dur- ation</i> (min)	$H_{m0,inc}$ (m)	$\frac{H_{m0,inc}}{h}$ (-)	$\frac{h}{L_{p,swell}}$ (-)	$\frac{h}{L_{p,sea}}$ (-)	$\frac{H_{m0,i}}{L_{p,sea}}$ (%)	M_{sw} (-)	$m_{0,swell}$ (10^{-6} m^2)	$m_{0,sea}$ (10^{-6} m^2)	Φ_{sw} (-)	$f_{p,swell}$ (Hz)	$f_{p,sea}$ (Hz)
1 – unimodal	20	0.089	0.148	-	0.194	2.9	-	-	497	-	-	0.65
2 – mildly bimodal	20	0.087	0.145	0.071	0.207	3.0	0.10	49	429	0.59	0.28	0.68
3 – moderate bimodal	20	0.089	0.148	0.074	0.222	3.3	0.20	99	391	0.59	0.29	0.72
4 – moderate bimodal	20	0.081	0.135	0.097	0.316	4.3	0.26	106	306	0.59	0.37	0.90
5 – extreme bimodal	20	0.075	0.125	0.109	0.375	4.7	0.55	199	157	0.59	0.41	0.99
6 – moderate bimodal, long experiment	90	0.093	0.155	0.05	0.26	4.1	0.21	114	424	0.75	0.20	0.8

4 Application and validation of wave pressure and wave force

This section presents the validation of the spectral LWT using the conducted experiments. Empirical response functions are evaluated by using the wave force spectrum, wave pressure spectrum, and the wave spectrum. The wave spectrum and wave force spectrum are given in section 4.1. The empirical pressure-response is given in section 4.2 and compared to the theoretical response functions. The calculated wave pressure profiles and the measured wave pressure profiles are evaluated in section 4.3. The same approach is applied for the wave force. The validation of the force response is given in section 4.4, the validation of the wave force in section 4.5. The validation of the probability distribution of the wave force is given in section 4.6.

4.1 Wave spectra and wave force spectra

From the experiments described in section 3, the wave spectra and wave force spectra are derived. The wave spectra are shown by the continuous lines in Figure 7; the left axis presents the wave variance density. In the same figure, the wave force spectra are indicated by the dashed lines. The right axis presents the wave force variance density. For

experiment 1 (unimodal) the peak of the force variance density is located lightly to the left compared to the peak of the wave variance density. Left form the peak frequency, the dashed line representing the force variance density exceeds the wave variance density. Right form the peak frequency, the force variance density falls below the wave variance density. Hence, an equal amount of wave variance density at low frequencies gives a higher amount of force variance density. This effect is more prominent for bimodal wave spectra. The wave variance density of the first peak amplifies more compared to the wave variance density of the second peak. This effect can be explained by the shape of the response function as described in section 2.2. This effect is amplified by the quadratic relationship between the wave spectrum and wave force spectrum (equation 8). The shape of the response function and the amplification by the quadratic relation gives a higher contribution of low frequency wave variance density to the wave force variance density compared to a same amount of wave variance density at higher frequencies. This can be demonstrated by experiment 4 and 5 of which the results are shown in Table 2. Experiment 4 and 5 are moderate and extreme bimodal and are identified by two peak frequencies. A unit value of wave variance density at the swell peak frequency generates more force variance density compared to a unit value of wave variance density at the sea peak frequency.

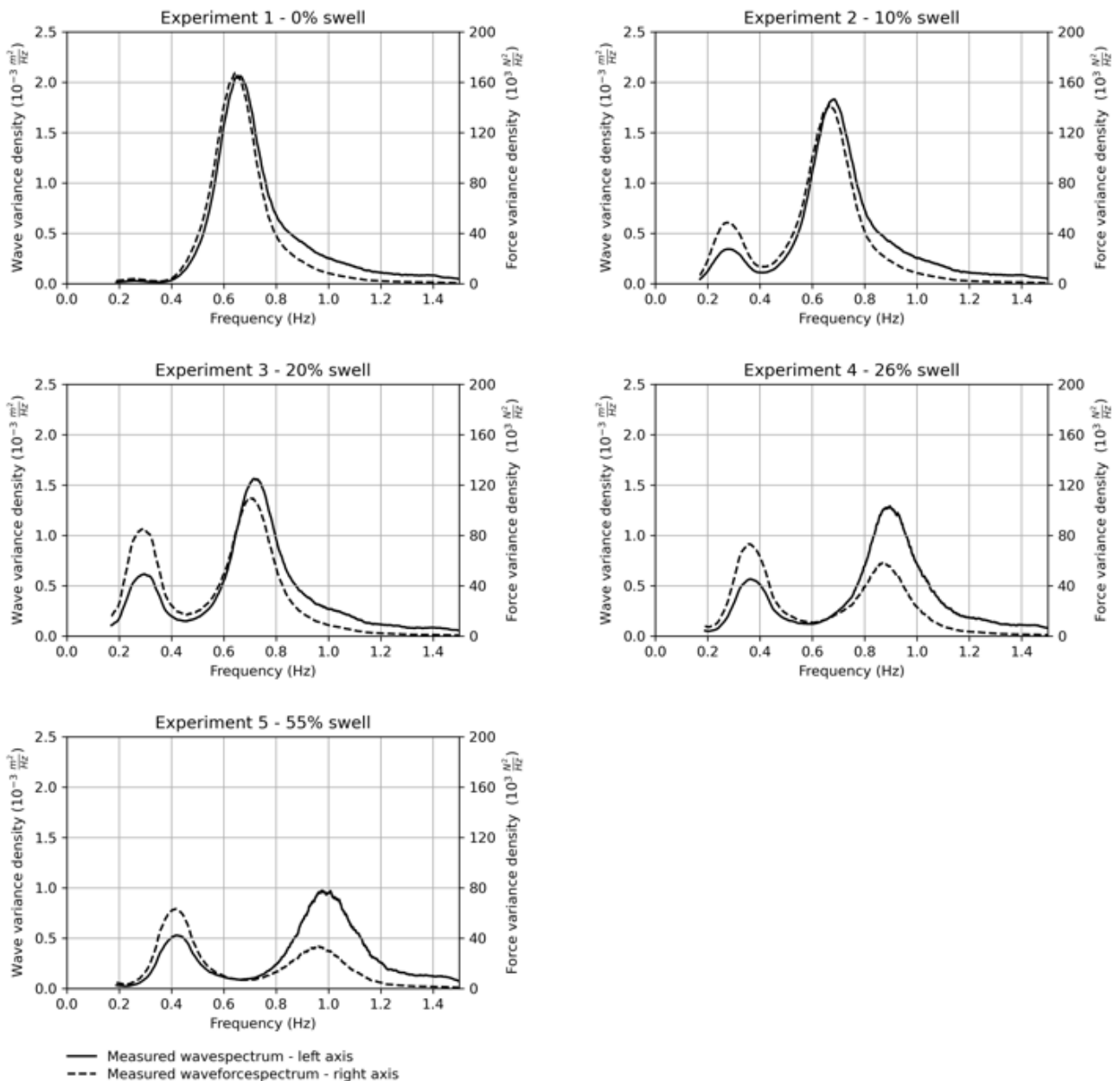


Figure 7: Wave spectra and wave force spectra.

Table 2: Comparison between wave variance density and force variance density

	Peak frequency	Wave variance density ($10^{-3} \text{ m}^2/\text{Hz}$)	Force variance density ($10^3 \text{ N}^2/\text{Hz}$)	Ratio Wave variance density : Force variance density ($1 \text{ m}^2/\text{Hz} : 10^6 \text{ N}^2/\text{Hz}$)-
Experiment 4	Swell	0.56	73	1:130
	Sea	1.28	58	1:45
Experiment 5	Swell	0.54	64	1:118
	Sea	0.97	33	1:34

4.2 Validation of pressure response

Pressure-response functions are derived for the five experiments given in Table 1. The empirical pressure response is derived by using equation 18:

$$R_{\eta p, \text{empirical}}^2(f, z) = \frac{S_{\eta\eta, \text{flume}}(f)}{S_{pp, \text{flume}}(f, z)} \tag{18}$$

where $S_{\eta\eta, \text{flume}}$ is the wave spectrum obtained by a FFT analysis of the gauge measurements, and $S_{pp, \text{flume}}$ is the wave force spectrum obtained by a FFT analysis of the force on the wall.

The theoretical pressure response as defined by equation 5 representing four pressure sensor that remain under water throughout the test (PS2, PS3, PS4, and PS5) are given by black lines in Figure 8. Each black line is representing a level below SWL. Sensors located above the troughs of the waves runs dry resulting in a lack of data during a wave through which makes the sensors PS7, PS10, and PS11 not applicable for this analysis. The empirical pressure response is shown by the colored areas in Figure 8. The colored areas correspond to the 95% confidence interval derived using the student's t distribution ("Student" (W.S. Gosset), 1908) of the pressure response at each depth representing one unimodal wave spectrum and four bimodal wave spectra. The pressure-response function and the empirical pressure-response are made dimensionless. The theoretical nondimensional response runs from 2 (due to nearly 100% reflection) and decreases for an increasing frequency as described in chapter 2.

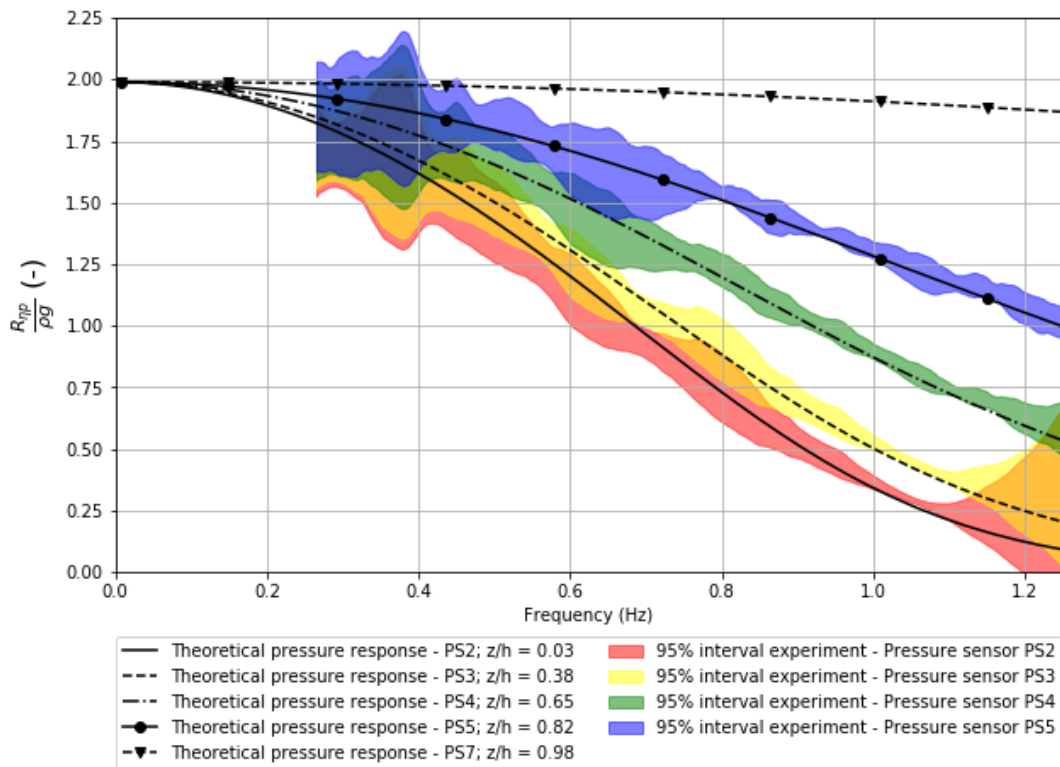


Figure 8: Pressure responses. The empirical response is derived from the experiments listed in Table 1.

The pressure response is the largest near SWL as expected, which can be seen by the dimensionless response of pressure sensor PS5. This sensor is located just below the troughs of the waves. The pressure response is less at greater depths which can be seen in the decrease of pressure responses for an increasing depth. PS2 is located just above the bottom of the wave flume. This sensor shows the lowest pressure-response.

The theoretical pressure response and the empirical pressure shows a good agreement for every frequency and depth. The accuracy decreases for frequencies lower than 0.4 Hz. This can be explained by the lack of wave variance density in the experiments for lower frequencies. A good match is found between 0.4 Hz and 1.1 Hz which corresponds to peak frequency of the second peak of the bimodal spectrum. A less accurate match is obtained for frequencies above 1.1 Hz due to the lack of variance density for experiment 1, experiment 2, and experiment 3.

4.3 Validation of wave pressure

In this section, the pressure profiles are compared to the various equations for pulsating wave loads. From the experiments, wave pressure profiles are derived for the waves corresponding to $F_{1/3}$ and the $F_{5\%}$. The significant wave height H_s is a commonly used variable, therefore the $F_{1/3}$ from the timeseries has been assessed as reference. Due to the duration of the experiments data for the ‘extreme’ values of wave forces is scarce. Therefore, $F_{5\%}$ is used as a representative ‘high’ force. For bimodal spectra, the peak frequency has been chosen for the peak with the highest amount of wave variance density. In engineering practice this would be the peak frequency of the wave spectrum representing the sea state to be used in the ‘traditional’ formulae. Under this assumption, kh ranges between 1.2 and 2.4.

The measured pressure profile, indicated by the red dots in Figure 9, corresponds to a 5% exceeded wave force ($F_{5\%}$) which is evaluated by using a PoT analysis. The red dots represent the measured wave pressures at sensor PS2, PS3, PS4, PS5, PS7 and PS9 (shown in Figure 5). When $P_{5\%}$ would have been used instead, a pressure profile would be composed of multiple waves. For example, a combination of a $P_{5\%}$ at the bottom and $P_{5\%}$ near SWL will not represent a pressure profile of one single wave. An error bar shows the nearest wave pressure (one higher and one lower with respect to the pressure profile of $F_{5\%}$) to indicate some scatter around the measured pressure profile. Figure 9 presents the wave pressure profiles corresponding to the characteristics shown in Table 1.

The most unfavorable matches are obtained by the formula of Sainflou and Goda-Takahashi. In these formulae, the pressure below SWL is schematized as a linear line ranging from SWL down to a pressure defined at the bottom. This linear approach of the pressure below SWL (0.6 m) does not match the measured wave pressures. Van Vledder (2019) and van Maris (2018) predicted this underestimation of Goda-Takahashi for unimodal wave spectra for the relative depth and relative wave steepness valid for the performed experiments. The formula of Sainflou gives a major overestimation for a unimodal wave spectrum over the full water column. For bimodal wave spectra, Sainflou gives an overestimation at SWL down to two third of the water depth. From the bottom up to one third of the depth of the flume, Sainflou underestimates the wave pressure.

The other formulae represent the pressure profile quite well for experiments 1 (unimodal) and 2 (10% relative swell). The quasi regular LWT performs less well for experiment 3 and gives a wrong wave pressure profile for experiment 4 and 5. This shows that this theory is not valid for bimodal sea states, as it does not account for the low frequency waves that penetrate further to the bed. The spectral LWT, New Wave LWT, and the squared sum of two Quasi-Regular LWT give a good approximation of the shape of the profile. Although the New Wave LWT underestimates the pressures somewhat near the bed for an increasing swell component with respect to the spectral approach.

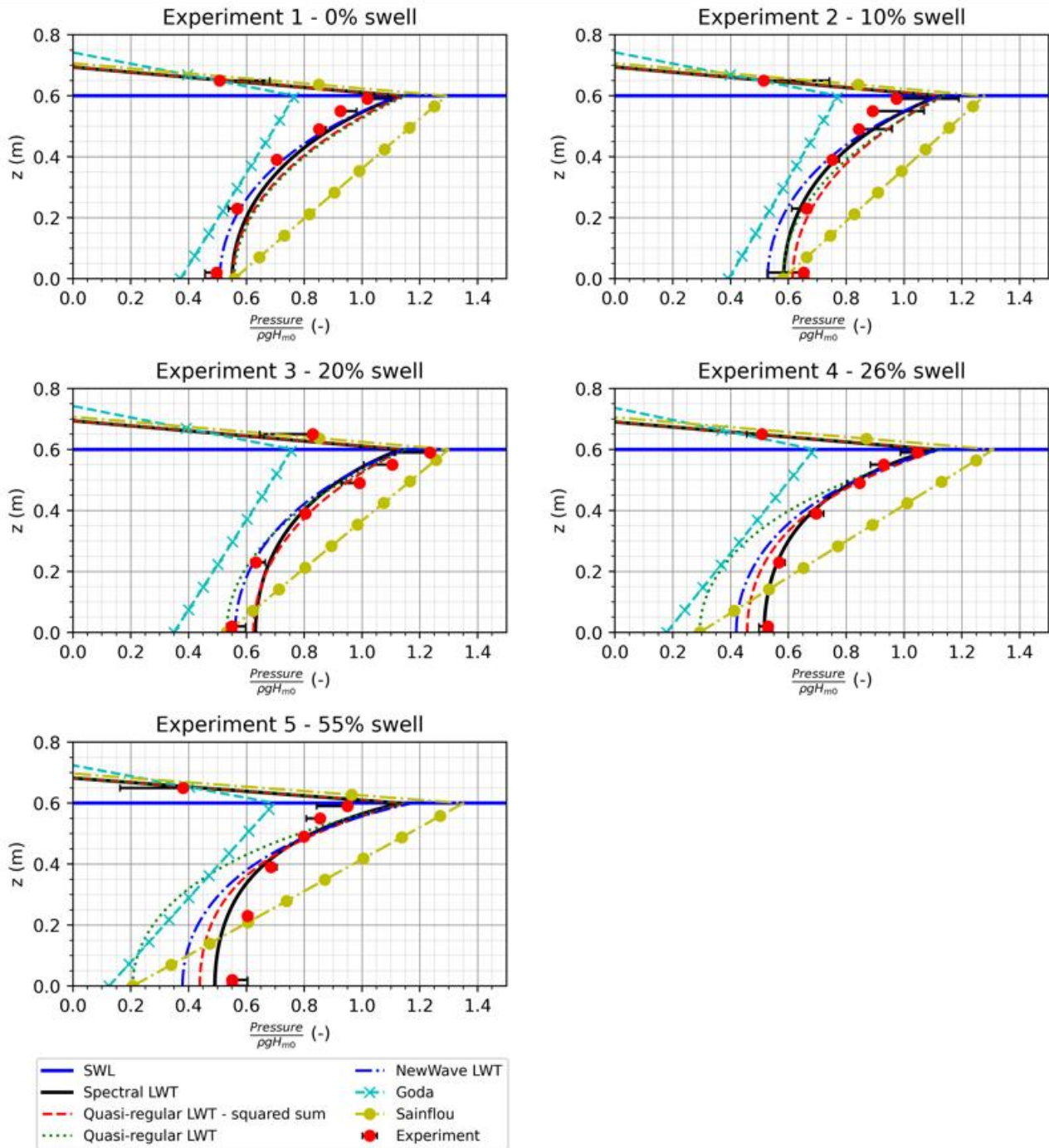


Figure 9: Wave pressure profiles – 5% probability of exceedance of the wave force.

Figure 10 provides a comparison between the measured pressure and computed wave pressure for every formula and for every experiment for a pressure profile corresponding the $F_{1/3}$ and $F_{5\%}$. The coefficient of determination (R squared) is given in the graphs and Table 3. The error between the calculated pressure and measured pressure is dependent of the actual measured wave pressure for Goda-Takahashi and experiment 4 and 5 for the basic linear wave theory.

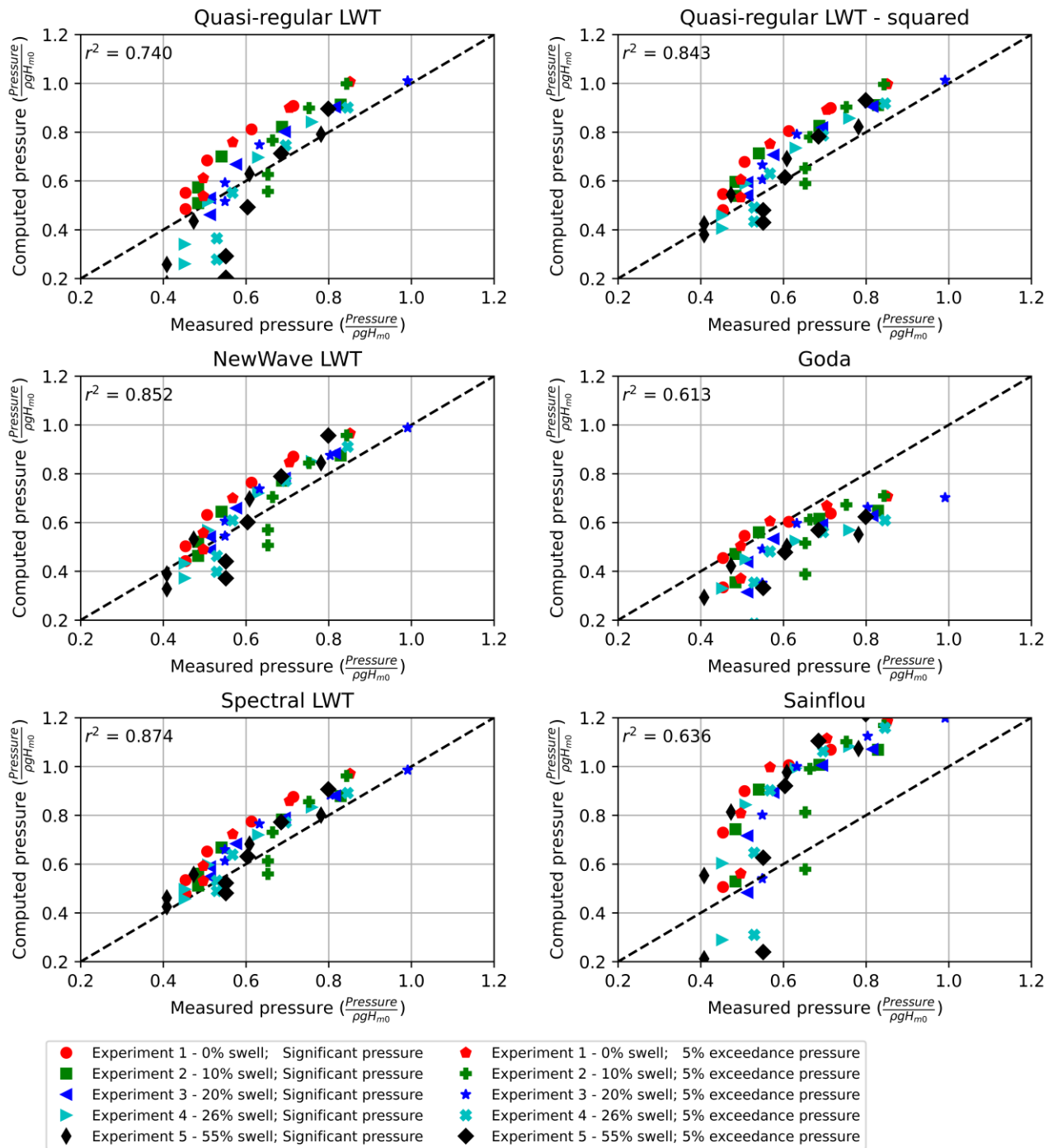


Figure 10: Accuracy of wave pressure models, measured pressures, and computed pressures

Table 3: Coefficient of determination per wave model for measured and calculated wave pressures.

Wave model	R^2
Quasi-regular LWT	0.740
Quasi-regular LWT – squared sum	0.843
New Wave LWT	0.852
Goda-Takahashi	0.613
Spectral LWT	0.874
Sainflou	0.636

The performance of the Quasi-Regular LWT is good for a unimodal and mild bimodal sea state (experiment 1 and 2). For moderate bimodal spectra (experiment 3 and 4) and high bimodal spectra (experiment 5) the performance of the Quasi-Regular LWT is poor. This can be seen by the pressure profiles and results given in Figure 10. The Quasi-Regular LWT gives an underestimation of pressures for bimodal wave spectra.

Goda-Takahashi gives an underestimation of nearly each pressure and is not suitable for the relative depth applied in the experiments. The formula does not seem to be applicable for a representative evaluation of pulsating wave forces for bimodal seas of limited steepness.

The overestimation of Sainflou is clearly visible in Figure 10. For the unimodal and mild bimodal sea state, the pressures are overestimated. For more bimodal seas the pressure at the bottom is underestimated. The triangular shape of the Sainflou pressure profile does not represent the actual pressure profile. This results in an overly conservative estimation of pressures. Therefore, the formula does not appear to be sufficiently accurate for design.

The error of the quasi-regular squared sum LWT, New Wave LWT, spectral LWT is quite constant for the range of measured pressures. The best match is found for the spectral LWT. The error is also constant for an increasing swell component. The New Wave LWT gives a slight underestimation for bimodal seas and has a slightly greater error compared to the spectral LWT. For the New Wave LWT the scatter for bimodal seas is larger compared to the spectral LWT. The quasi-regular squared sum LWT gives a good indication of the wave force for bimodal seas when using two peak periods and wave heights. Hence, these formulae are applicable for an approximation of the wave pressure profile for bimodal seas as concluded previously.

4.4 Validation of force response

In this section the empirical force response is validated using the same methodology as used for the empirical pressure response. The total theoretical response is calculated using equation 10. The results are shown by the black lines in Figure 11. The empirical results for the five wave spectra given in Table 1 and Figure 7 are shown by the colored areas given in Figure 11. The colored areas correspond to the 95% confidence interval derived using the student's t distribution ("Student" (W.S. Gosset), 1908) representing one unimodal spectrum and four bimodal spectra. For the total response (blue area) the empirical responses of the unimodal and bimodal spectra are indicated by the grey lines. The response is made dimensionless by dividing the response by ρgh . The dimensional response per running meter below SWL starts at a value of 2 and decreases to 0 for an increasing wave frequency. The nondimensional response above SWL is modelled by a constant value. This value is independent from the wave frequency and depends only on the reflection and water depth as described in section 2.

The match between the empirical total response indicated by the blue area and the theoretical total response indicated by the continuous line is fair, with a consistent overestimation of the theoretical value of about 10%. The confidence is less good for frequencies below 0.4 Hz due to the limited amount of variance density in the applied wave spectra in the experiments. A similar match is obtained for the response below SWL, as it constitutes a major part of the force variance. The empirical response above SWL gives a stable result over the whole frequency domain and corresponds to the linearized response as given in equation 12 for $\gamma_{lin} = 1.0$.

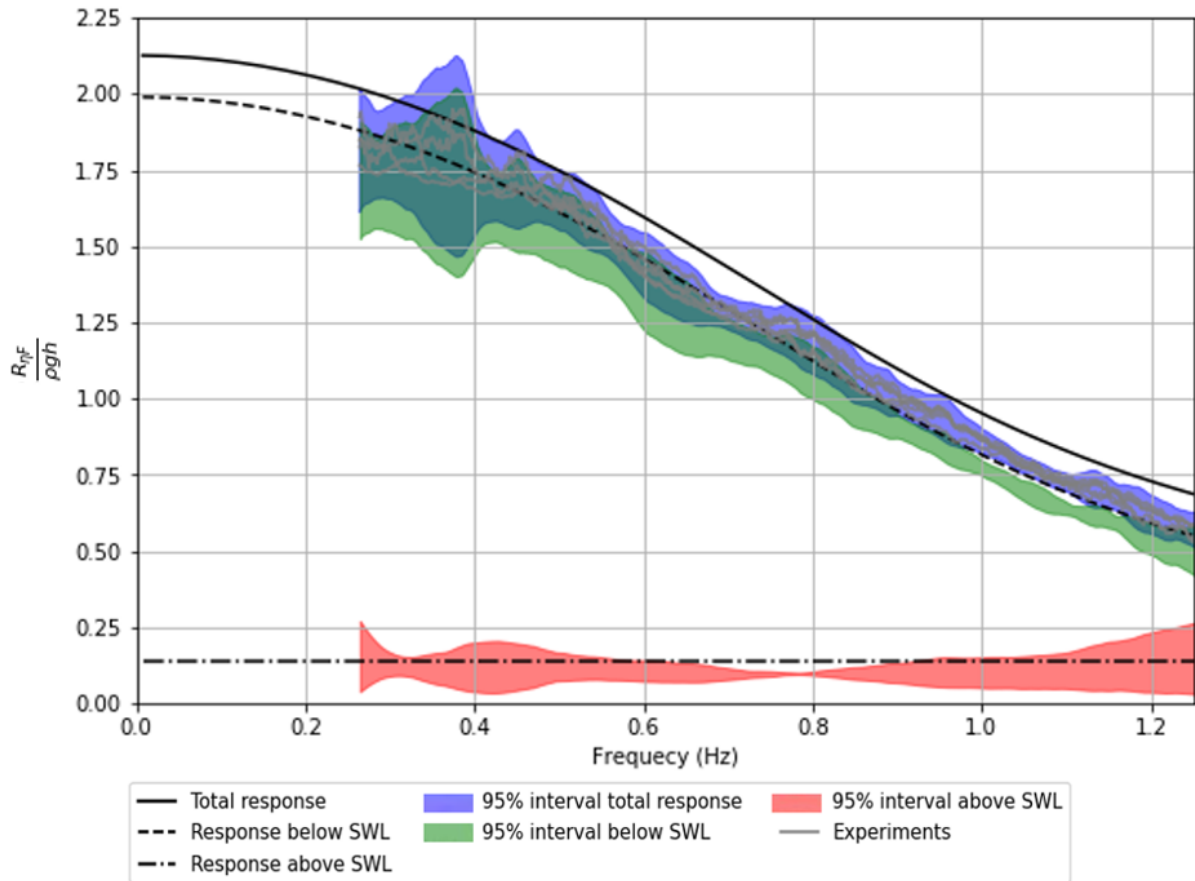


Figure 11: Response below water level, Response above water level, and total response (t-distribution; 95% confidence interval of 5 experiments (Table 1))

4.5 Validation of wave force

Figure 12 presents the relative difference between the total wave force as predicted by the wave formulae compared to the measured F_s and $F_{5\%}$ of the presented five experiments. For the traditional formulae the peak frequency of the highest component of the wave spectrum has been applied. The relative force differences on the vertical axis are given as a function of the relative swell presented on the horizontal axis.

The spectral LWT coincides best with the measured forces. It slightly underestimates the force for the bimodal seas, increasing with M_{sw} up to an underestimation of nearly 6% for experiment 5. The New Wave LWT shows a similar resemblance, but slightly less accurate with 14% underestimation for experiment 5. The quasi-regular squared sum LWT gives a significant overestimation for a low relative swell but a reasonably good estimate for an increasing amount of swell. The quasi-regular LWT gives a reasonable approach up to a relative swell of $M_{sw} = 0.2$, with deviations up to 12%. Goda-Takahashi gives a significant underestimation as discussed in previous chapters. Sainflou overestimates the force with 39% for $M_{sw} = 0$ and overestimates the force for the tested range of bimodal seas.

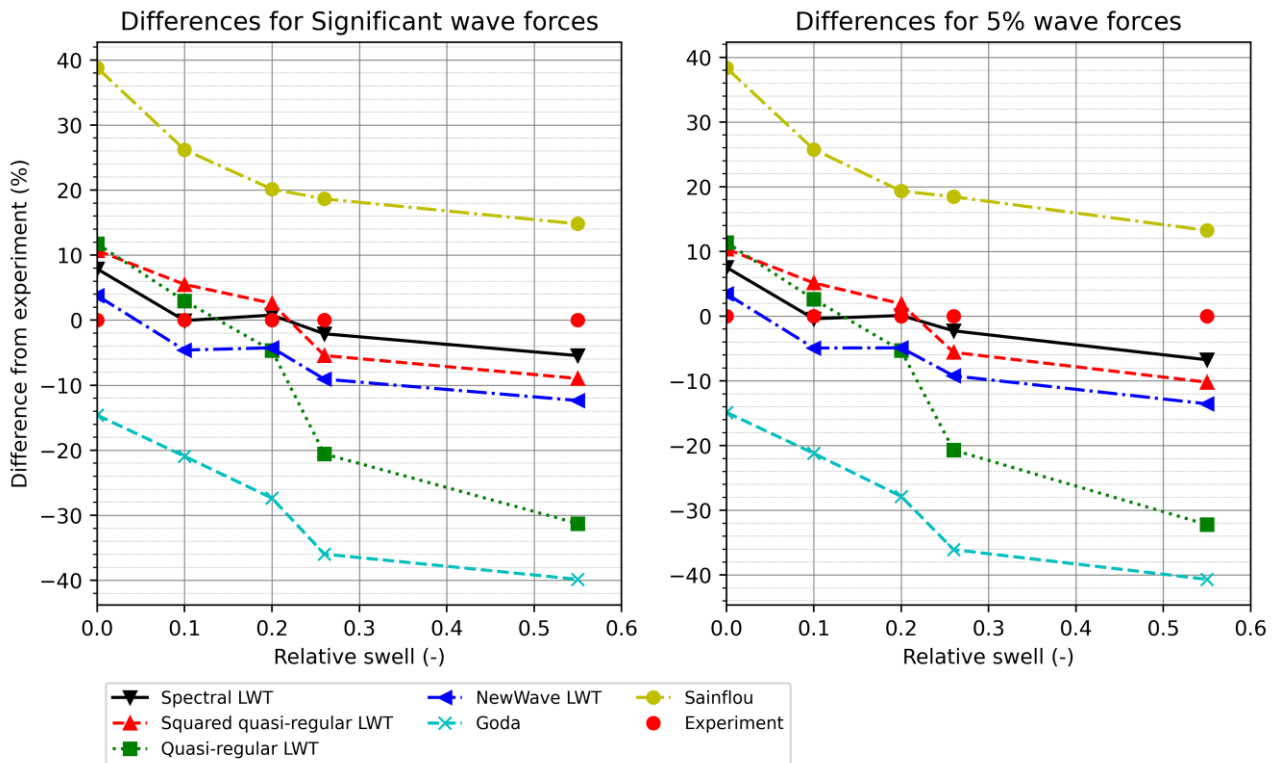


Figure 12: Difference between theoretical wave force and measured wave force for an increasing relative swell.

4.6 Validation of probability distribution of wave forces

For the design of hydraulic structures, a design wave must be defined which is representative for the observed sea state. As stated in the introduction, Guedes Soares (2012) concluded that the Rayleigh and Weibull distributions yield a good fit in almost all ranges of bimodal seas. These distributions can also be applied to the wave force generated by bimodal seas. Within this section, the probability of exceedance of the measured wave forces is compared to the Rayleigh distribution.

As stated in section 2.3, the design wave can be evaluated using the significant wave force derived from the wave force spectrum. The wave force spectrum can be derived from two sources:

- The theoretical wave force spectrum derived from the wave spectrum (continuous line in Figure 7) and the response function (equation 10).
- The measured wave force spectrum obtained by a FFT analysis (dashed line in Figure 7).

The wave force probability distribution is found by using the significant wave force as a scale parameter in the Rayleigh distribution (equation 15). The exceedance distributions of the five experiments are shown in Figure 13. Measured wave forces are indicated by the red crosses, the probability distributions using the wave spectra are shown based on the theoretical wave force spectrum (green dash-dotted lines) and measured significant force (blue dashed lines). Both methods give a good representation of the probability distribution both for unimodal sea states (experiment 1) and bimodal sea states. The use of the wave spectrum gives a conservative approach due to the upper limit approach of the response function as shown in Figure 11.

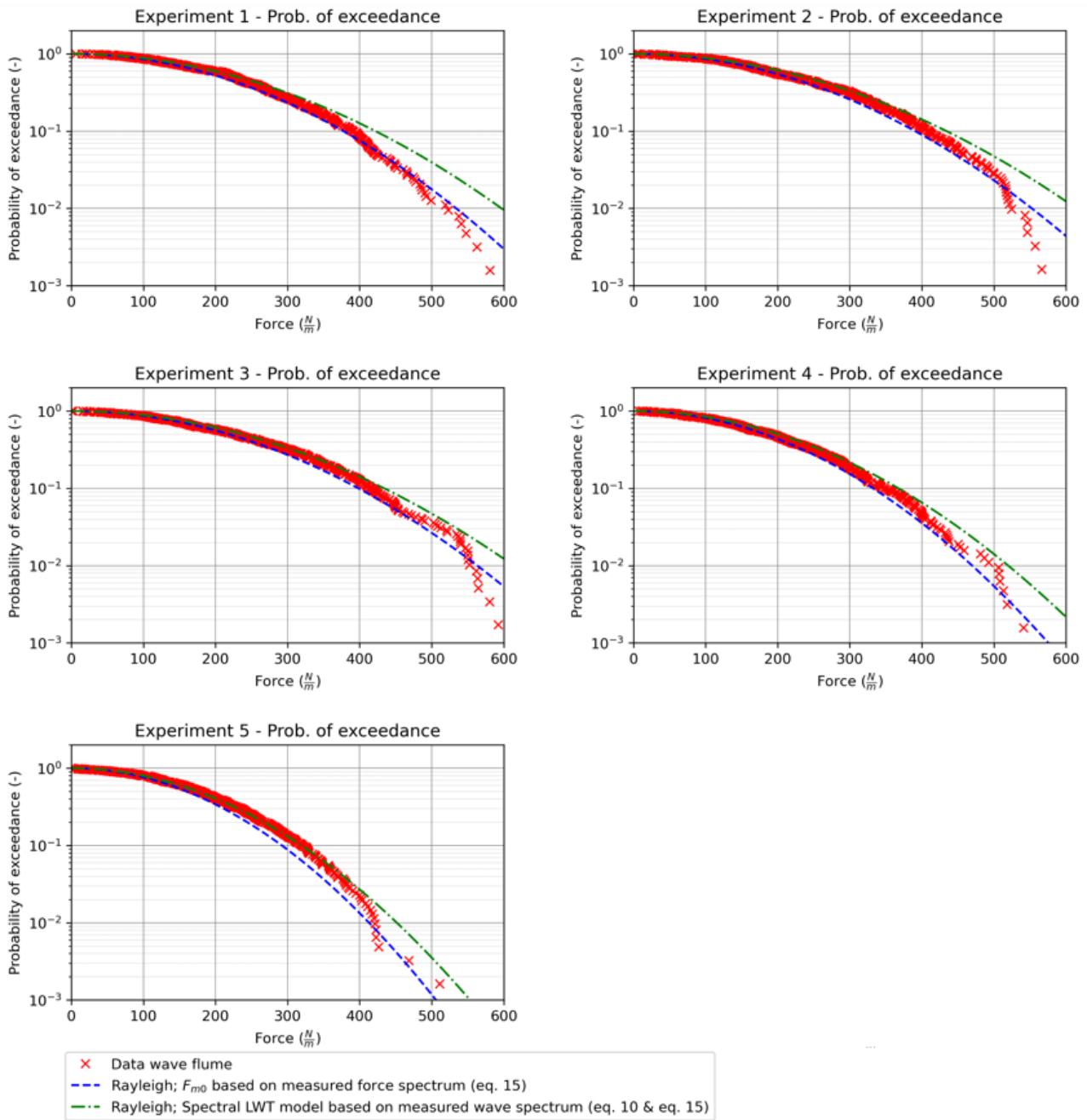


Figure 13: Probability of exceedance of wave forces, force below SWL

The duration of the time series of experiments shown in Figure 13 is limited, hence the range of probabilities of the conducted experiments is limited. One long experiment has been conducted of which the result is shown in Figure 14. The accuracy for low probabilities for this experiment is better as it has a lower sampling error. In this graph it seems that the exceedance curve based on the wave spectrum gives a better fit to the data.

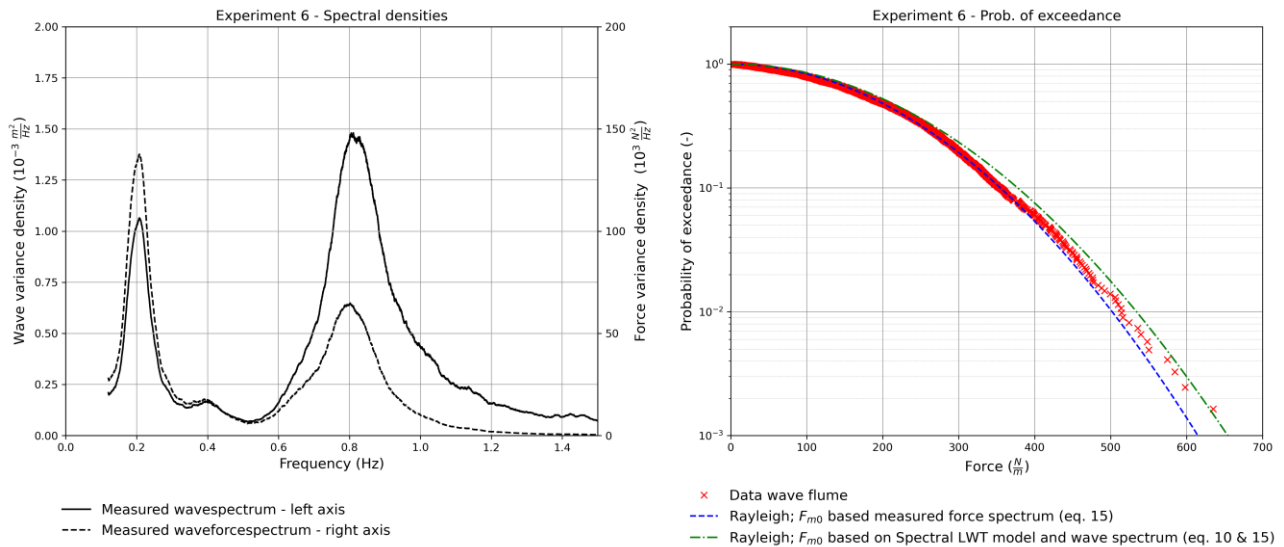


Figure 14: Wave spectra, wave force spectra, and probability of exceedance of wave forces for experiment 6.

5 Discussion

The presented methodologies are based on the LWT. However, in many wave conditions waves are nonlinear. The impact on the accuracy of nonlinearity on the results of the flume tests is discussed in section 5.1 and 5.2. Section 5.3 discusses the validity of the formula of Goda-Takahashi. Many designers are inclined to use this formula assuming it is conservative to do so. However, as shown in the present analysis of the model tests and numerical investigation (Van Vledder 2019 and Van Maris 2019), the formula is not conservative in some cases. A nondimensional comparison is made between the formula of Goda-Takahashi and the Quasi-regular LWT, spectral LWT, and New Wave LWT.

5.1 Nonlinear effects and ‘double humps’

Due to higher order wave effects, the peak of a wave will flatten and a ‘double hump’ in the wave pressure, wave force, or water level elevation develops (Goda, 1966). The magnitude of the ‘double hump’ will be the largest for the highest recorded waves in a time series, as these will be steeper and hence be more nonlinear. Goda (1966) made a classification of nonlinear effects based on the relative depth and wave steepness. This classification is applied to experiment 1 (unimodal, 0% swell energy) and experiment 5 (bimodal, 55% swell energy) The results are shown in the last row of Table 4.

Table 4: Relative depth, wave steepness and expected nonlinear effects of the 2% of exceedance waves, based on zero-crossing period and height.

	Experiment 1	Experiment 5
2% wave height ($1.4 * H_{m0,inc}$) (Rayleigh distribution)	0.132 m	0.116 m
Highest wave frequency	0.65 Hz	0.99 Hz
Relative depth	0.19 (-)	0.38 (-)
Wave steepness	0.042 (-)	0.074 (-)
Nonlinear effects on wave pressures, forces, and crest shape (Goda, 1966)	Between ‘Double humps at bottom’ and ‘Double humps on total force’	‘Double humps at MWL’

Figure 15 shows the recorded wave force and the wave pressure at the bottom for a wave corresponding to a 2% probability of exceedance. A clear ‘double hump’ is visible for the wave pressure at the bottom which corresponds to prior publications (Goda, 1966; Le Méhauté 1976). The above-mentioned non-linear effects are present in the wave time series and force time series applied for the validation of the LWT for every experiment. However, the impact of non-

linear effects on the values of the peak pressures and peak wave forces for irregular broad banded wave spectra is limited as shown in Figure 13. Further investigation is required for assessing the maximum range of wave steepness and the effect on the accuracy of the calculated force or pressure based on the (spectral) linear wave theory.

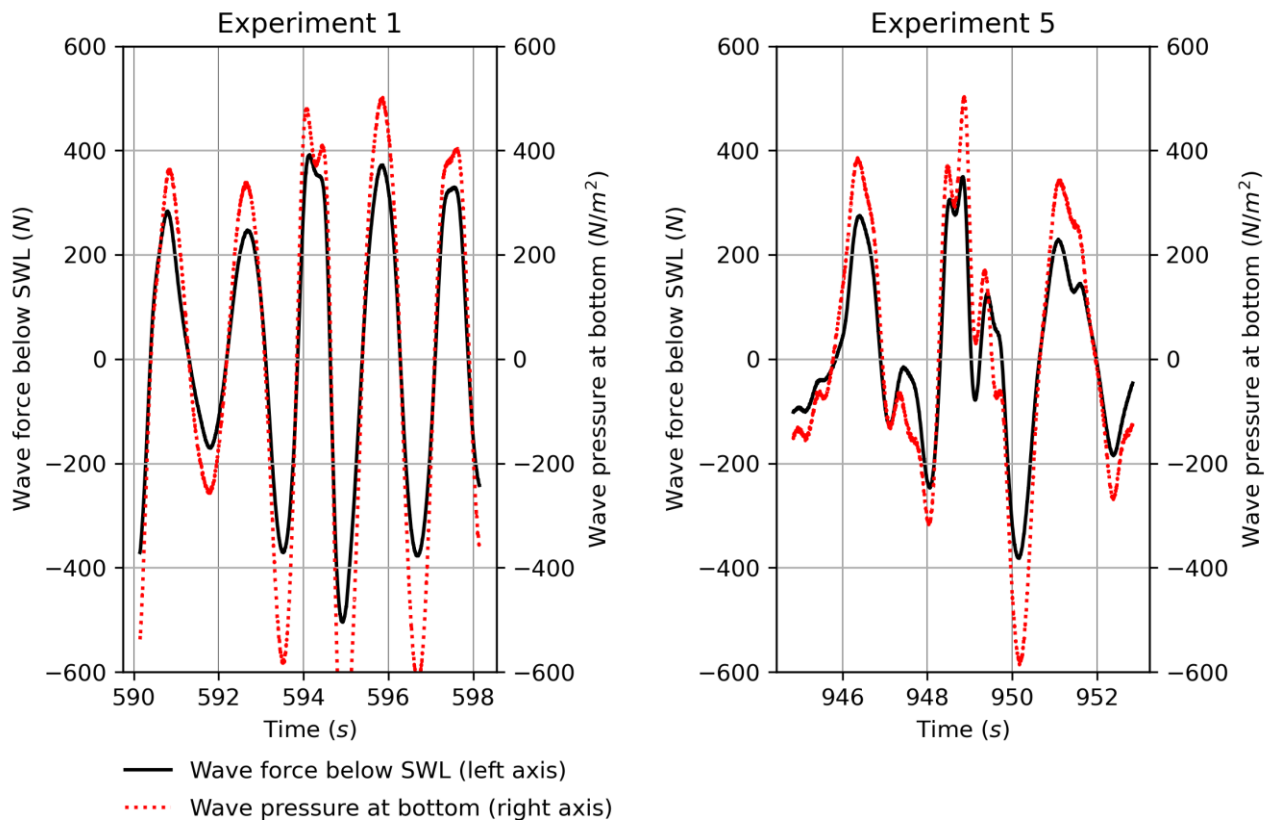


Figure 15: Wave force and wave pressure corresponding to a 2% probability of exceedance wave.

5.2 Evaluation of recorded time series – mean water elevation

An increase in mean water level for a standing wave profile at the antinode near a wall are given by Sainflou (1928) and Miche (1944). This increase in water level also gives an increase in the wave force at a vertical wall. Figure 16 presents the recorded wave force of experiment 1 (unimodal, 0% swell energy) and experiment 5 (bimodal, 55% swell energy). A 100.0 s moving average is applied to identify the long-term water level variations. The moving average (black line) of the wave force at the wall of each experiment is greater than zero and shows limited fluctuations. This could be explained by the force due to mean water level elevation as identified by Sainflou. The dashed red line in Figure 16 represents the wave force due to the mean water level elevation as described by Sainflou (1928), as given by δ_0 in the CEM (USACE, 2011). The magnitude of the force of the mean water elevation force is calculated using $H = H_{m0}$ and $T = 1/f_{p,sea}$. The match between the moving average and calculated force due to mean water elevation is quite good and stable for the wave forces for a unimodal and bimodal spectrum.

The force due to mean water elevation at the wall corresponds to 5% of the total force for the unimodal experiment and 8% for the experiment 5 (55% swell). This increase of force is limited and within the accuracy of the applied method as shown in Figure 13. Note that its value is already included in the measured peak values that are compared to the various formulas in section 4. More investigation is required for the assessment of mean water elevation for unimodal and bimodal seas.

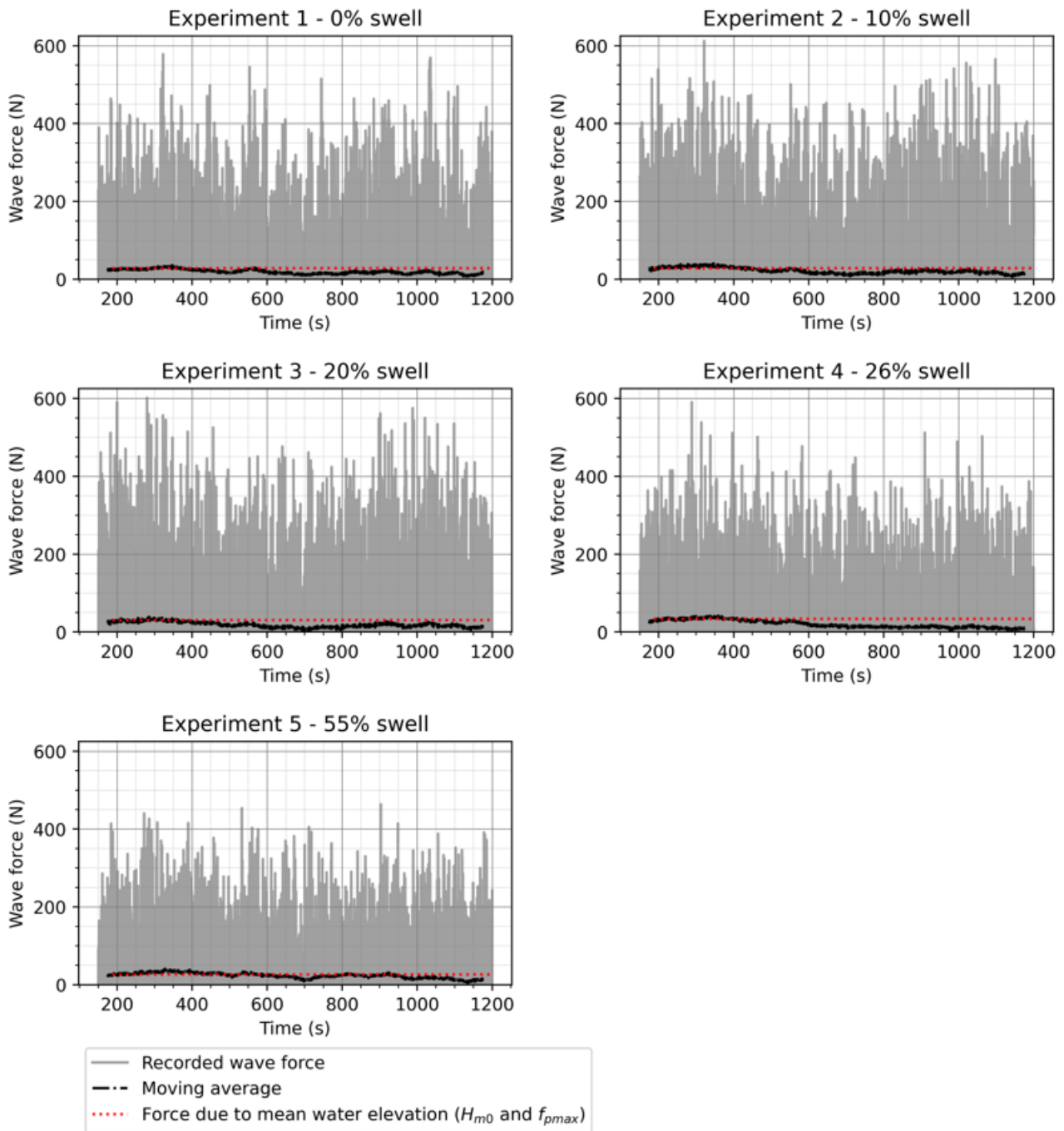


Figure 16: Recorded wave force time signal including moving average and the calculated force due to mean water elevation.

5.3 General comparison of wave force formulae for unimodal sea states

Multiple wave formulae for regular or unimodal wave fields have been assessed in this paper. A theoretical comparison of the outcome of the formulae has been performed. The results are shown in Figure 17. The outcome of the formula of Goda-Takahashi, Sainflou, and multiple variants of the LWT are shown in a dimensionless form at the left section of Figure 17. The forces below SWL are considered to provide a dimensionless comparison between the formulae. The force above SWL is not included in the graph due to the quadratic dependency on the wave height. The force below SWL according to the formula of Sainflou cannot be represented by a single line due to the quadratic relationship between the wave amplitude and the mean water elevation. Therefore, the force below SWL according to Sainflou is given for: $H_{m0_inc}/d = 0.05, 0.1, \text{ and } 0.15$.

The right side of Figure 17 shows a comparison of LWT formulae and the formula of Goda-Takahashi, and Sainflou ($H_{m0_inc}/d = 0.15$ representing the conducted wave flume experiments). For the NewWave LWT and spectral LWT a standard JONSWAP spectrum (Hasselmann, 1973) is applied. A different shape of the spectrum results in a different outcome of the presented results. The following can be concluded based on Figure 17:

1. The formulae based on the LWT show a similar pattern, the Quasi-regular LWT is the most conservative. The spectral LWT and New Wave LWT are less conservative for a unimodal spectrum.
2. The formula of Sainflou corresponds to the other LWT formulae up to $k_p h = 1.0$ and generates a conservative estimation of the wave force. For higher values, the formula is less applicable due to the overconservative values of the wave force with respect to the other formulae.
3. The formula of Goda-Takahashi performs well for $k_p h \lesssim 0.5$ which corresponds to the range of tests performed by Goda (1972). These wave conditions correspond to a wave field exerting maximum load at breakwaters at shallow conditions. For this range, the LWT theories underestimate the load.
4. Goda-Takahashi underestimates for the range of $0.5 \lesssim k_p h \lesssim 2.5$ compared to LWT. This underestimation is also found in the experiments and in the SWASH analysis (van Vledder 2019) and (Van Maris 2019). Hence this underestimation seems to be realistic.
5. Goda-Takahashi overestimates the wave force for $k_p h \gtrsim 2.5$. For this range, small waves and large water depths are present. The wave pressure does not penetrate over the full water column and the wave pressure will be zero somewhere between SWL and the bottom. Goda-Takahashi assumes a linear pressure profile and equals zero at the bottom. This assumption yields to a significant overestimation.

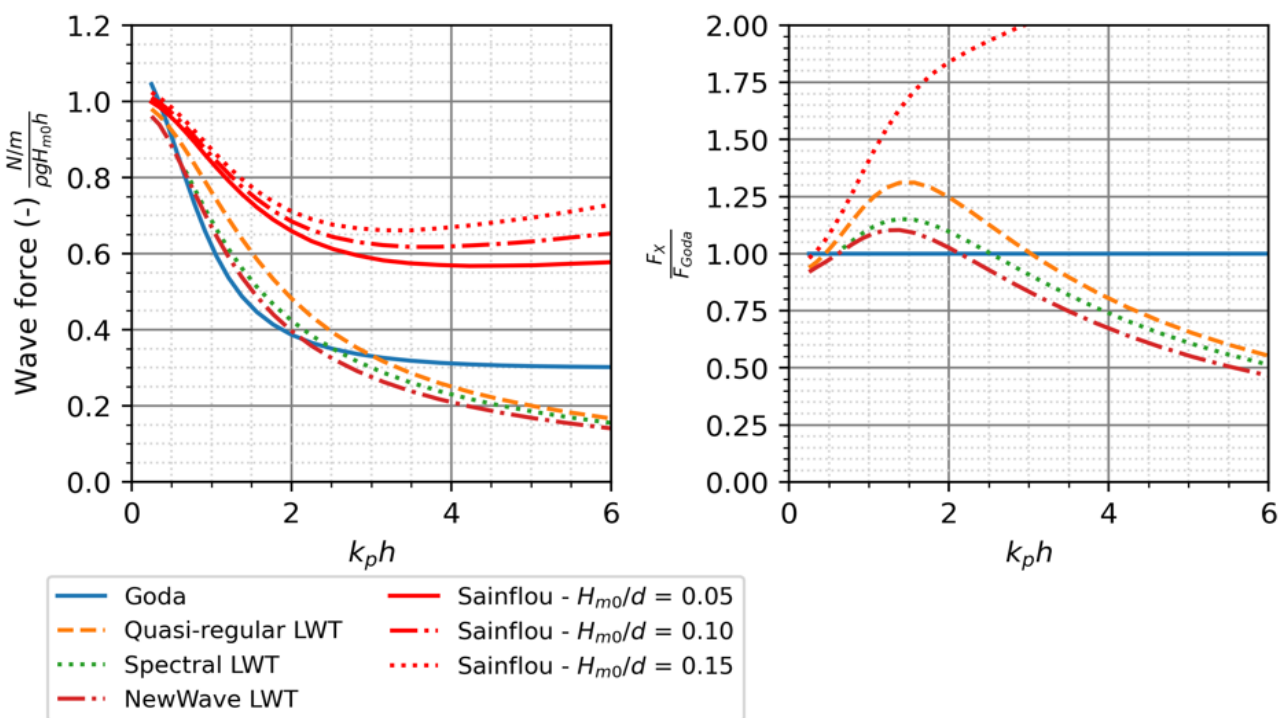


Figure 17: Comparison between wave force formulae below SWL for 100% reflection. NOTE: results of spectral LWT and New Wave LWT are dependent on the shape of the wave spectrum.

6 Conclusions

This paper validates of the spectral LWT using wave flume experiments and the assessment of the performance of multiple wave force formulae for unimodal and bimodal wave spectra.

Experiments were conducted in a wave flume for unimodal and bimodal wave spectra up to a steepness of 7.4%. The outcome of the wave flume experiments, and the accuracy of general formulae have been compared. The spectral LWT

model has been validated using the wave flume experiments. The validation shows a good agreement for unimodal (0% swell energy) and bimodal (up to 55% swell energy) wave spectra for the response functions, pressures, and probability distribution. The match between the empirical response functions and wave pressures and forces to the theoretical response functions forces and pressures is good. The conclusions described in this paper are drawn upon five short and one long experiment. Future research covering multiple wave flume tests per wave spectrum running from unimodal up to extreme bimodal seas will increase the accuracy of the presented validation.

Nonlinear effects like ‘double-humps’ and elevated mean sea level have been observed. However, the nonlinear effects had minor impact on the accuracy of the values of characteristic peak load determined by the spectral linear theories. Use of a higher-order non-linear wave theory using a quasi-regular assumption is not expected to lead to a better, and probably worse, prediction of peak forces for bimodal sea states.

Spectral LWT and New Wave LWT are well applicable for both unimodal and bimodal broad banded wave spectra. These theories use an arbitrary wave spectrum as input and do not depend on only one wave height and wave period. A linearization factor γ_{lin} for the pressure above SWL equal to 1.0 (-) gives a conservative result for the pressure response. This yields a conservative result for wave forces. Both formulae can estimate a wave force generated by a broad-banded wave spectrum with sufficient accuracy. However, the New Wave LWT gives limited information about the contribution of a certain wave frequency to the total wave pressure or wave force. The spectral LWT provides this information in the shape of a force spectrum or pressure spectrum. This insight of the contribution of a certain frequency to the total wave force or pressure is of great added value of the spectral LWT for the design of large hydraulic structures as prior described. This insight gives the designer more information and sensibility of the structure to certain wave frequencies. The probability distribution of wave forces is estimated well for the tested broad banded bimodal wave spectra using a Rayleigh distribution and the spectral LWT. The use of the significant force as scale parameter gives a good match between the probability distribution obtained from wave flume data and the applied formula.

A model accounting for the spectral shape is recommended for the evaluation of wave forces and wave pressures on vertical walls loaded by broad banded or bimodal wave spectrum. The spectral LWT and the New Wave LWT perform well. Traditional formulae like the formula of Goda-Takahashi, Sainflou, or quasi-regular LWT should be used with care for limited swell components (up to 20% swell energy).

The pressure profiles of Goda-Takahashi represent the total force well for low values of $k_p h$ but are less applicable for the design of hydraulic structures (lock gates, weirs, barriers, drive mechanism) located on a horizontal bed. For the design of these structures, the pressure profile near SWL could dominates the loads on steel parts, drive mechanism, gate supports, etc. A formula representing the pressure profile the best should be chosen for design. Global analysis of stability of breakwaters and other hydraulic structures (founded on a berm or horizontal bed) should also be checked using Goda-Takahashi formula.

For conditions with greater relative depth and high values of $k_p h$ as tested in the experiment and bimodal seas, Goda-Takahashi and Sainflou should not be used. The impact on the wave force of limited swell energy increases for an increasing depth as shown by the shape of the response functions. For bimodal seas the quasi-regular LWT can be applied instead of the traditional quasi-regular LWT by applying a quadratic sum of two pressure profiles (one corresponding to swell component and the one corresponding to the sea component of the spectrum).

At last, a comparison is made between wave force formulae for unimodal wave spectra. The prior described wave formulae are derived for specific conditions. The common wave force formulae are mainly derived for regular waves or unimodal narrow spectrum. The following can be concluded for the accuracy of the formulae for a range of $k_p h$:

- For low values of $k_p h$ ($k_p h \lesssim 0.5$) for structures located on a horizontal bed and on a berm, the formula of Goda-Takahashi should be used. The formula of Goda-Takahashi has been developed for shallow water conditions ($k_p h < 0.5$) and (near) breaking waves for the global analyses of the stability of breakwaters (sliding and overturning) and gives a conservative result. The formula of Goda-Takahashi accounts for breaking waves for geometries with a berm at the toe of the hydraulic structure. This aspect is not incorporated for formulae using LWT
- For moderate values of $k_p h$ ($0.5 \lesssim k_p h \lesssim 2$ up to 3) spectral LWT seems best suited for structures on a horizontal bed. For this range, spectral LWT approach is conservative with respect to Goda-Takahashi, and realistic, according to the presented experiments. For $k_p h = 0.5$ up to 1.0 Goda-Takahashi should be used

with care, the rate of conservatism depends on the spectral shape. For the wave pressures of the unimodal spectrum tested in the wave flume ($k_p h = 1.22$) Goda-Takahashi underestimated the pressure profile below SWL and underestimated the total wave force by 12%.

- For high values of $k_p h$ ($k_p h > 2$ to 3) a formula based on the LWT is best suited. The formula of Goda-Takahashi has not been developed for this range and gives an overly conservative estimate of the wave force for nonbreaking waves. This overly conservative estimate yields from the triangular schematization of the wave force below SWL.
- The formula of Sainflou can be used as conservative approach up to ($k_p h \lesssim 1.0$). Sainflou is over-conservative with respect to the other formulae for higher values of $k_p h$.

Acknowledgements

The authors would like to thank Delft University of Technology for the use of the wave flume for this research. It was a great opportunity to use the test setup which was part of the DynaHicS (Dynamics of Hydraulic Structures) project. The first author would also offer his thanks to the Hydraulic Engineering department of Arcadis The Netherlands BV for making time and resources available for this research.

Author contributions (CRediT)

HT¹: Conceptualization, Literature study, Analysis, Data analysis of time series, Formal Analysis, Investigation, Methodology, Software, Validation, Visualization, Writing – original draft, Writing – review & editing. BH²: Methodology of NewWave and higher order wave loads, Writing – Review, Supervision. HV³: Methodology, Writing – Review, Supervision. EdA⁴: Wave flume experiments, Data analysis, Visualization of experimental setup, Writing – Review .

Notation

Name	Symbol	Unit
Wave amplitude	a	m
Reference wave amplitude, used for linearization, $= \frac{1}{2}\gamma_{lin}H_{m0}$	a_{ref}	m
Frequency	f	Hz
Peak frequency of the swell spectrum	$f_{p,swell}$	Hz
Peak frequency of the wind sea spectrum	$f_{p,sea}$	Hz
(peak) force	F	N/m
Force per unit of width calculated by New Wave theory	F_{NW}	N/m
Significant force per unit of width; the average third-highest peak forces of all incoming Waves	$F_{1/3}$	N/m
Force per unit of width due to the swell part of the spectrum	$F_{LWT,swell}$	N/m
Force per unit of width due to the wind sea part of the spectrum	$F_{LWT,sea}$	N/m
Significant force per unit of width	F_{m0}	N/m
Peak force per unit of width exceeded by x% of the incoming waves	$F_{x\%}$	N/m
Gravitational acceleration	g	m/s^2
Water depth	h	m
Wave height of single wave	H	m
Extreme design wave height	H_d	m
Unreflected wave height.	$H_{m0,inc}$	m
Discretization step of wave spectrum based on wave number	Δk	m^{-1}
Wave number	k	m^{-1}
Wave number pertaining to the design wave and local wavelength	k_d	m^{-1}
Wave number pertaining to peak frequency and local wavelength	k_p	m^{-1}
Wavelength	L	m
(local) wavelength corresponding to $f_{p,sea}$	$L_{p,sea}$	m
(local) wavelength corresponding to $f_{p,swell}$	$L_{p,swell}$	m
Relative swell variance	M_{sw}	
Zeroth order moment of spectrum, equal to variance of signal	m_0	m^2

Name	Symbol	Unit
Wind sea variance (total variance above the frequency with the minimum between the swell and wind peaks in the spectrum)	$m_{0,sea}$	m^2
Swell variance (total variance density between 0Hz and the minimum between the swell and wind peaks in the spectrum)	$m_{0,swell}$	m^2
Pressure	p	N/m^2
Pressure at water line	p_1	N/m^2
Significant pressure; the average third-highest peak pressures of all incoming waves	$P_{1/3}$	N/m^2
Significant pressure	P_{m0}	N/m^2
Peak pressure exceeded by x% of the incoming waves	$P_{x\%}$	N/m^2
Reflection coefficient, ratio of reflected to incoming significant wave height	r	-
Force-response per unit of width	$R_{\eta F}$	N/m^2
Force-response per unit of width above SWL	$R_{\eta F,top}$	N/m^2
Force-response per unit of width below SWL	$R_{\eta F,sub}$	N/m^2
Pressure-response above SWL	$R_{\eta p,top}$	N/m^3
Pressure-response below SWL	$R_{\eta p,sub}$	N/m^3
Wave steepness based on local wavelength and peak period	S_p	-
Wave steepness based on fictitious deep-water wavelength and peak period	S_{op}	-
Variance density spectrum of force per unit of width	S_{FF}	$N^2/(m^2 Hz)$
Wave spectrum, a.k.a. variance density spectrum of water surface elevation	$S_{\eta\eta}$	m^2/Hz
Variance density spectrum of pressures	S_{pp}	$N^2/(m^4 Hz)$
Significant wave period (average period of the periods corresponding to the highest one third of waves)	$T_{1/3}$	s
Wave period corresponding to peak of the wave spectrum	T_p	s
Vertical coordinate relative to seabed	z	m
Vertical elevation of top of structure	z_{top}	m
Factor in Goda's formula representing the berm geometry and impulsive wave loading.	α_1	-
Factor in Goda's formula representing the berm geometry and impulsive wave loading.	α_2	-
Water level setup at wall according to Sainflou	δ_0	m
Empirical factor for linearization of force induced by wave crest ($z > h$)	γ_{lin}	-
Relative swell peak frequency	Φ_{sw}	-
Mass density of water	ρ	kg/m^3

References

- Airy, G., 1845. Tides and waves. London, Encyclopaedia Metropolitana.
- Akbari, H., Panahi, R., Amani, L., 2019. A double-peaked spectrum for the northern parts of the Gulf of Oman; revisiting extensive field measurements data by new calibration methods. *Ocean Engineering* 180, 187-190
- Akbari, H., Panahi, R., Amani, A., 2020. Improvement of double-peaked spectra: Revisiting the combination of the Gaussian and the JONSWAP models. *Teheran, Ocean Engineering* 198
- Arcadis the Netherlands BV, 2020. GOLFBELASTINGEN VISSERIJSLUIS OOSTENDE - VAST DEEL; Toepassing spectrale lineaire golftheorie.
- Chen Yan-Yih, Hsu Hung-Chu, 2009. A third-order asymptotic solution of nonlinear standing water waves in Lagrangian coordinates. *Taiwan, China, Chinese Phys.* B15 861
- De Almeida, E., Hofland, B., 2020 Validation of pressure-impulse theory for standing wave impact loading on vertical hydraulic structures with short overhangs. *Delft, Coastal Engineering* 159.
- Goda, Y., Fukumori, T., 1972. Laboratory investigation of wave pressures exerted upon vertical and composite walls. *Nagase Yokusaka Japan, Rept. Port and Harbour Res. Inst. (in Japanese)*.
- Goda, Y. 1974. New wave pressure formulae for composite breakwaters. *Proc. Int. Conf. on Coastal Eng. ICCE. Copenhagen, Denmark.* <https://doi.org/10.9753/icce.v14.100>
- Goda, Y., Kakizaki, S., 1966. Study on finite amplitude standing waves and their pressures upon a vertical Wall. *Japan, Rept. Port and Harbour Res. Inst. (in Japanese)* 5 (10)
- Goda, Y., Design of upright breakwaters. *Proc. Int. Conf. on Design and Reliability of Coastal structures. ICCE. Venice, Italy.*
- Goda, Y., 2010. *Random seas and design of maritime structures.* 3rd edition. World scientific

- Guedes Soares, C., Carvalho, A.N., 2012. Probability distributions of wave heights and periods in combined sea-states measured off the Spanish coast. Lisboa, Portugal, *Ocean Engineering* 52 (2012) 13-21
- Hasselmann K., T.P. Barnett, E. Bouws, H. Carlson, D.E. Cartwright, K. Enke, J.A. Ewing, H. Gienapp, D.E. Hasselmann, P. Kruseman, A. Meerburg, P. Miller, D.J. Olbers, K. Richter, W. Sell, and H. Walden. Measurements of wind-wave growth and swell decay during the Joint North Sea Wave Project (JONSWAP) *Erganzungsheft zur Deutschen Hydrographischen Zeitschrift Reihe, A*(8) (Nr. 12), p.95, 1973.
- Holthuijsen, L., 2007. *Waves in Oceanic and Coastal Waters*. Cambridge: University Press.
- Le Méhauté, B., 1976, *An Introduction to Hydrodynamics and Water Waves*, New York, Springer-Verlag, 315 pp.
- Longuet-Higgins, M.S., 1952. On the statistical distributions of the eight of sea waves, *J. Mar. Res.*, 11, 3, 245-265
- Mulder, T., Vrijling, J.K., 1980. Probabilistic load determination. Delft, The Netherlands, Delft University Press – Technical aspects related to the design of the Oosterschelde Storm Surge Barrier in the Netherlands – Volume 1 section II Design philosophy and strategy in the project related research
- Paprotta, M., 2021. Nonlinear standing water waves generated in a closed numerical flume, *Ocean Engineering* 219 (2021) 108326
- Penney, W.G., Price, 1952. A.T., Part II. Finite periodic stationary gravity waves in a perfect liquid. *Philosophical Transactions of the Royal Society of London. Series A, Mathematical and Physical Sciences* Vol. 244, No. 882, 254-284
- Petrova, P.G., Guedes Soares, C., 2011. Wave height distributions in bimodal sea states from offshore basins. Lisboa Portugal, *Ocean Engineering* 38, 658-672
- Romanczyk, W., 2007. Instability of nonlinear standing waves in front of a vertical wall. Rimouski; Canada, *Journal of Fluids and Structures* 23 733-753.
- Rijkswaterstaat, 2018. *Werkwijzer Ontwerpen Waterkerende Kunstwerken – Ontwerpverificaties voor de hoogwatersituatie. Groene versie 2018 (In Dutch) Version D2. RWS-WVL Waterkeringen. Ministry of Water Management and Infrastructure.*
- Sainflou, M., 1928. *Essai sur les diques maritimes verticaux*. Paris, Technical report.
- Sobey, R. J. (2009) Analytical solutions for steep standing waves. *Proc. of the Institution of Civil Engineers. Eng. and Comp. Mechanics* 162. Dec.2009 Issue EM4. pp 185–197 doi: 10.1680/eacm.2009.162.4.185.
- "Student" (W.S. Gosset), "The probable error of a mean" *Biometrika* , 6 (1908) pp. 1–25
- Tadjbakhsh, I., 1960. Keller, J.B., Standing surface waves of finite amplitude. *Journal of Fluid Mechanics*, 8 (03) 442-451.
- Tromans, P.S., Anaturk, A.R., Hagemeyer, P., 1991. A new model for the kinematics of large ocean waves— applications as a design wave. *Proceedings of the 1st International Offshore and Polar Engineering Conference, Edinburgh*, vol. 3, pp. 64–71.
- Tuin, H.G., Voortman, H.G., Wijdenes, T., van der Stelt, W., van Goolen, D., van Lierop, P., Lous, L., Kortlever, W., 2018. Spectral analysis of wave forces for the design of rolling gates of the lock of Amsterdam. Panama City, PIANC; World Congress Panama City.
- USACE, 2011. *Coastal Engineering Manual – Part VI*. Washington, DC 20313-1000.
- van Maris, B., 2018. Wave loads on vertical walls – Validation of design methods for non-breaking waves of bimodal spectra. Delft, Delft University of Technology
- van Vledder, G. P., Hofland, B., Tuin, H.G., van Maris, B., 2019. Numerical evaluation of design rules for non-breaking wave loads on vertical walls. Karlsruhe, Bundesanstalt für Wasserbau. S. 762-772
- Vlaams Nederlandse Scheldecommissie, 2017. *Hydraulische Randvoorwaarden*.
- Voortman, H.G., Wijdenes, T., Tuin, H.G., van der Stert, W., van Lierop, P., Lous, L., Kortlever, W., 2017. Hydraulic loads on a large lock gate. *ICE 2017: Coasts, Marine Structures and Breakwaters 2017: Realising the Potential*
- Vrijling, J.K., Janssen, J.P.F.M., Bruinsma, J., 1983. A practical method to obtain wave and storm surge conditions for predictions and probabilistic calculations. *North Sea Dynamics*. Springer Berlin Heidelberg. 233-247
- Zelt, J.A., Skjelbreia, J.E., 1992. Estimating incident and reflected wave fields using an arbitrary number of wave gauges. Venice Italy, *Proc. Coastal engineering conference 1992*